Jefferson Lab PAC 26

Proposal Cover Sheet

JLAB USER GROUP

This document must be received by close of business Monday,

May 24, 2004 at:

Jefferson Lab
User/International Liaison
Mail Stop 12B
12000 Jefferson Ave
Newport News, VA
23606

[Lab's choice]
Experimental Hall: C (smallest uncertainty) and A

Days Requested for Approval: 25

Proposal Title:

The Neutron Electric Form Factor at $Q^2 = 4.3$ (GeV/c)^2 from the Reaction $^2H(\vec{e}, e'\vec{n})^1H$ via Recoil Polarimetry

Proposal Physics Goals

Indicate any experiments that have physics goals similar to those in your proposal.

Approved, Conditionally Approved, and/or Deferred Experiment(s) or proposals:

E02-013 for G_E^n/G_M^n at Q^2 up to 3.4 (GeV/c)^2

Contact Person

Name: Richard Madey

Institution: Kent State University & Jefferson Lab

Address: Kent, OH 44242 &

Address: Newport News, VA 23606

City, State, ZIP/Country: USA

Phone: (757)-269-7323 **Fax:** (757)-269-6273

E-Mail: madey@jlab.org

Jefferson Lab Use Only

Receipt Date:____________________________________

By:____________________________________

LAB RESOURCES LIST

JLab Proposal No.: ____________________ Date May 23, 2004

(For JLab ULO use only.)

List below significant resources — both equipment and human — that you are requesting from Jefferson Lab in support of mounting and executing the proposed experiment. Do not include items that will be routinely supplied to all running experiments such as the base equipment for the hall and technical support for routine operation, installation, and maintenance.

Major Installations *(either your equip. or new equip. requested from JLab)*

- Neutron Polarimeter & Enclosure
- Dipole Magnet (Charybdis)
- Steel Shadow Shield
- Lead Curtain

New Support Structures:

- Shield House & Collimator for Polarimeter
- Support Structure for Polarimeter
- Support Structure for Shadow Shield

Data Acquisition/Reduction

Computing Resources:

New Software:

Major Equipment

Magnets*:*
- HMS
-Charybdis (with tapered pole tips)

Power Supplies*:*
- HMS
- SOS (for Charybdis)

Targets*:*
- LD2
- LH2
- Dummy

Detectors*:*
- Additional Detectors for Polarimeter
- Replacement PMTs for Polarimeter Detectors

Electronics*:*
- Quad Constant-Fraction Discriminators
- Delay Lines
- Multihit TDC's

Computer Hardware*:*

Other*:*
- Moeller Polarimeter
- Compton Polarimeter, if available

Other:

BEAM REQUIREMENTS LIST

JLab Proposal No.: ____________ Date: May 23, 2004

Hall: C and A   Anticipated Run Date: ____________   PAC Approved Days: ____________

Spokesperson: Richard Madey   Hall Liaison: ____________
Phone: (757)-269-7323
E-mail: madey@jlab.org

List all combinations of anticipated targets and beam conditions required to execute the experiment. (This list will form the primary basis for the Radiation Safety Assesment Document (RSAD) calculations that must be performed for each experiment.)

Condition No.	Beam Energy (MeV)	Mean Beam Current (μA)	Polarization and Other Special Requirements (e.g., time structure)	Target Material (use multiple rows for complex targets — e.g., w/windows)	Material Thickness (mg/cm^2)	Est. Beam-On Time for Cond. No. (hours)
1	6000	100	>= 80% Polarization	15-cm LD2	2430	528
2	6000	100	>= 80% Polarization	15-cm LH2	1065	17
3	6000	1	>= 80% Polarization	Fe	8	24
4	6000	10	>= 80% Polarization	15-cm LD2	2430	12
5	6000	100	>= 80% Polarization	Al	583	7

The beam energies, E_{Beam}, available are: $E_{Beam} = N \times E_{Linac}$ where N = 1, 2, 3, 4, or 5. E_{Linac} = 800 MeV, i.e., available E_{Beam} are 800, 1600, 2400, 3200, and 4000 MeV. Other energies should be arranged with the Hall Leader before listing.

HAZARD IDENTIFICATION CHECKLIST

JLab Proposal No.: ____________________ Date: May 23, 2004

(For JLab U/I Liaison Office use only.)

Check all items for which there is an anticipated need.

Cryogenics
- [ ] beamline magnets
- [ ] analysis magnets
- [x] target

type: LD2, LH2
flow rate: ____
capacity: ____

Electrical Equipment
- [ ] cryo/electrical devices
- [ ] capacitor banks
- [x] high voltage
- [ ] exposed equipment

Radioactive/Hazardous Materials
List any radioactive or hazadorous/ toxic materials planned for use:

Pressure Vessels
- ____ inside diameter
- ____ operating pressure
- ____ window material
- ____ window thickness

Flammable Gas or Liquids
type: ____
flow rate: ____
capacity: ____

Drift Chambers
type: ____
flow rate: ____
capacity: ____

Other Target Materials
- [ ] Beryllium (Be)
- [ ] Lithium (Li)
- [ ] Mercury (Hg)
- [ ] Lead (Pb)
- [ ] Tungsten (W)
- [ ] Uranium (U)
- [ ] * Helium (^{3}He)
- [x] Other (list below)

- Aluminum Dummy
- Fe (for Moeller Polarimeter)

* U/I Liaison Office to notify RADCON

Vacuum Vessels
- ____ inside diameter
- ____ operating pressure
- ____ window material
- ____ window thickness

Radioactive Sources
- [ ] permanent installation
- [x] temporary use

type: 228 Thorium
strength: ~ 10 uC

Large Mech. Structure/System
- [ ] lifting devices
- [ ] motion controllers
- [x] scaffolding or
- [x] elevated platforms

Lasers
type: ____
wattage: ____
class: ____

Installation:
- [ ] permanent
- [ ] temporary

Use:
- [ ] calibration
- [ ] alignment

Hazardous Materials
- [ ] cyanide plating materials
- [ ] scintillation oil (from)
- [ ] PCBs
- [ ] methane
- [ ] TMAE
- [ ] TEA
- [ ] photographic developers
- [ ] other (list below)

General

Experiment Class:
- [ ] Base Equipment
- [ ] Temp. Mod. to Base Equip.
- [ ] Permanent Mod. to Base Equipment
- [x] Major New Apparatus

Other: Polarimeter

Computing Requirements List

Proposal Title: The Neutron Electric Form Factor at Q^2=4.3 (GeV/c)^2 from the Reaction ^2H(e,e'n)^1H via Recoil Polarimetry

Spokesperson: Richard Madey **Experimental Hall:** C and A

Raw Data Expected

Total: 1500 GB **Per Year (long duration experiments only):** ______

Simulation Compute Power (SPECint95 hours) Required: 2000 hours CPU on Linux farm

On-Line Disk Storage Required: 600 GB work space

Imported Data Amount from Outside Institutions: ______

Exported Data Amount to Outside Institutions:w ______

Expected Mechanism for Imported/Exported Data: ______

Special Requirements

For example, special configuration of data acquisition systems) that may require resources and/or coordination with JLab's Computer Center. Please indicate, if possible, what fraction of these resources will be provided by collaborating institutions and how much is expected to be provided by JLab.

Submit

Proposal to PAC 26

The Neutron Electric Form Factor at $Q^2 = 4.3$ (GeV/c)^2

from the Reaction $^2H(\vec{e}, e'\vec{n})^1H$ via Recoil Polarimetry

Spokesman: R. Madey, Kent State University

Co-Spokesman: S. Kowalski, MIT

Co-Spokesman: A. Yu. Semenov, Kent State University

Co-Spokesman: B. D. Anderson, Kent State University

Abstract

We propose to extend measurements of the electric form factor of the neutron, G_E^n, to a squared four-momentum transfer of 4.3 (GeV/c)^2, to achieve the same uncertainty [$\Delta G_E^n = 0.0020$] as that projected for the measurement with the polarized ^3He target at $Q^2 = 3.4$ (GeV/c)^2, and in a comparable beam time [25 days]. *This proposed measurement would represent the highest Q^2 for a G_E^n measurement anywhere and is achievable before the 12 GeV upgrade becomes a reality.*

The JLab E93-038 collaboration conducted $d(\vec{e}, e'\vec{n})p$ measurements on a liquid deuterium target at Q^2 values of 0.45, 1.13, and 1.45 (GeV/c)^2. *Polarization measurements above $Q^2 \approx 1$ (GeV/c)^2 require the beam energies available at CEBAF. In the technique demonstrated in E93-038 with a high-luminosity, high-efficiency neutron polarimeter and the dipole neutron-spin-precession magnet [Charybdis], we measured the ratio of two scattering asymmetries associated with positive and negative precessions of the neutron polarization vector.* In this ratio technique, systematic uncertainties are small because the analyzing power of the polarimeter cancels in the ratio, and the beam polarization cancels also because, as demonstrated in E93-038, the beam polarization does not change much in sequential measurements of the two scattering asymmetries.

The primary motivation for this measurement is the ability to measure a fundamental quantity of the neutron – one of the basic building blocks of matter. Because our method is sensitive to the sign of G_E^n, the proposed experiment will determine the sign of G_E^n in the region of 4 (GeV/c)^2, which is crucial for disentangling the structure of the nucleon. A successful model of confinement must be able to predict both neutron and proton electromagnetic form factors simultaneously. The neutron electric form factor is especially sensitive to small components of the nucleon wave function, and differences between model predictions for G_E^n tend to increase rapidly with Q^2. The proposed measurements of G_E^n will be available to distinguish models and to challenge rigorous Lattice QCD calculations. These measurements of G_E^n are needed to understand electron scattering experiments that probe electric structure functions at high Q^2; it is important for the analysis of few-body data from measurements at Jefferson Lab. Nuclear physics corrections [for FSI, MEC, and IC] are more reliable for the deuteron than for helium; also, the reaction mechanism is expected to be simpler in deuterium than in helium.

List of Participants

R. Madey (Spokesman), B.D. Anderson (Co-Spokesman and Institutional Representative), A.R. Baldwin, D.M. Manley, A.Yu. Semenov (Co-Spokesman), I.A. Semenova, J.W. Watson, W.-M. Zhang, Graduate Student

Kent State University

R. Carlini (Institutional Representative), R. Ent, H. Fenker, D. Gaskell, M. Jones, D. Higinbotham, A. Lung, D. Mack, B. Reitz, G. Smith, W. Vulcan, B. Wojtsekhowski, S. Wood, C. Yan

Thomas Jefferson National Accelerator Facility

S. Kowalski (Co-Spokesman and Institutional Representative), M. Farkhondeh, S. Taylor

Massachusetts Institute of Technology

C. Howell (Institutional Representative), S. Tajima, Postdoc

Duke University

H. Breuer, J.J. Kelly (Institutional Representative), N. Savvinov

University of Maryland

E. Crouse, J.M. Finn (Institutional Representative), C. Perdrisat

The College of William and Mary

O.K. Baker (Institutional Representative), E. Christy, L. Cole, P. Gueye, C. Keppel, L. Tang, A. Uzzle, L. Yuan, X. Zhu

Hampton University

A. Ahmidouch (Institutional Representative), S. Danagoulian, A. Gasparian

North Carolina A&T State University

G. MacLachlan, A. Opper (Institutional Representative)

Ohio University

List of Participants (continued)

R. Asaturyan, H.G. Mkrtchyan (Institutional Representative), T. Navasardyan, V. Tadevosyan

Yerevan Physics Institute

S. Wells (Institutional Representative), N. Simicevic

Louisiana Tech

P. Markowitz (Institutional Representative), B. Raue, J. Reinhold

Florida International University

D. Day (Institutional Representative), P. McKee

University of Virginia

W. Tireman

Pennsylvania State University at Erie

P.E. Ulmer

Old Dominion University

M. Khandaker (Institutional Representative), V. Punjabi, F. Wesselmann

Norfolk State University

M. Elaasar

Southern University at New Orleans

R.E. Segel

Northwestern University

R. Wilson

Harvard University

List of Participants (continued)

S. Jin, W.-Y. Kim (Institutional Representative), S. Stepanyan, S. Yang, Graduate Student

Kyungpook National University

T. Reichelt

University of Bonn

L. Gan

University of North Carolina at Wilmington

H. Arenhovel

University of Mainz

B. Plaster

California Institute of Technology

I. Sick

University of Basel

K. McCormick

Rutgers University

Contents

Page

List of Figures

List of Tables

1 Response to PAC25

This proposal is an improved version of the one that was deferred by PAC25. The proposal to PAC25 contained modest upgrades to the neutron polarimeter, which enabled us to measure G_E^n at $Q^2 = 3.0$ and 4.0 (GeV/c)^2 in 37 days with statistical uncertainties $\Delta G_E^n = 0.0034$. Now by increasing the vertical acceptance of the neutron polarimeter, we are able to measure G_E^n at a higher Q^2 [$Q^2 = \mathbf{4.3}$ (GeV/c)^2] in a shorter time [**25 days**] with a substantially smaller statistical uncertainty $\Delta G_E^n = \mathbf{0.0020}$. The systematic errors on the proposed measurements are estimated to be small, so that the total error would be completely statistics dominated. The previously-approved experiment 02-013 plans to use a polarized ^3He target to measure G_E^n up to 3.4 (GeV/c)^2 in 32 days with a projected total error of 0.0020 at $Q^2 = 3.4$ (GeV/c)^2, 0.0033 at $Q^2 = 2.4$ (GeV/c)^2, and 0.0047 at $Q^2 = 1.3$ (GeV/c)^2. We believe that the polarimeter configuration in our proposal to PAC26 permits the recoil polarimetry experiment to reach **the highest $\mathbf{Q^2}$ ever** for a G_E^n measurement and to achieve the level of statistical accuracy desired by PAC25.

Our proposed measurement at $Q^2 = 4.3$ (GeV/c)^2 is in a most interesting region. Extrapolation of our G_E^n data from E93-038 [together with the world data] indicates that G_E^n will be larger than G_E^p in the Q^2 region from 4.0 to 4.5 (GeV/c)^2; consequently, the isovector electric form factor [$G_E^v \equiv G_E^p - G_E^n$] would become negative. Such an observation would provide an additional constraint on models. Iachello and Bijker (2004) calculated the isovector electric form factor as a function of Q^2 and predicts that it becomes negative at about 3 (GeV/c)^2; a similar calculation by Miller (2002) predicts that the isovector electric form factor becomes negative at $\sim$4.3 (GeV/c)^2. Results from Bijker and Iachello (2004) and Miller (2002) are shown in Fig. 6 for the isovector electric form factor.

In summary, we have extended the Q^2 region [to $Q^2 = 4.3$ (GeV/c)^2] and expect the same small uncertainty [$\Delta G_E^n = 0.0020$] as projected for the ^3He measurement [E02-013] at 3.4 (GeV/c)^2 in a comparable beam time [25 days]. PAC25 acknowledged the importance of making complementary measurements for such a fundamental quantity as G_E^n.

2 Scientific Motivation and Background

2.1 Extension of E93-038 to Measure G_E^n at $Q^2 = 4.3$ (GeV/c)^2

The electric form factor of the neutron, G_E^n, is a fundamental quantity needed for the understanding of both nucleon and nuclear structure. The dependence of G_E^n on Q^2 reflects the distribution of charge in the neutron. The E93-038 collaboration carried out measurements of G_E^n from September 8, 2000 to April 26, 2001 at three values of Q^2 [viz., 0.45, 1.13, and 1.45 (GeV/c)^2]. Results were reported in Physical Review Letters [Madey et al. (2003)], which is Appendix A of this proposal. Data from E93-038 are plotted (as filled squares) in Fig. 1 together with the current world data extracted from polarization measurements [Eden et al. (1994), Herberg et al. (1999), Bermuth et al. (2003), Golak et al. (2001), Passchier et al. (1999), Zhu et al. (2001)] and from an analysis of the deuteron quadrupole form factor [Schiavilla and Sick (2001)]. We fitted these data and the G_E^n slope at the origin as measured via low-energy neutron scattering from electrons in heavy atoms [Kopecky et al. (1997)] to a Galster et al. (1971) parameterization:

$$G_E^n = -a\mu_n \tau G_D/(1 + b\tau), \tag{1}$$

where $\tau = Q^2/4M_n^2$, $G_D = (1 + Q^2/\Lambda^2)^{-2}$, and $\Lambda^2 = 0.71$ (GeV/c)^2. Our best-fit parameters are a = 0.886±0.023 and b = 3.29±0.31 [Kelly (2003)].

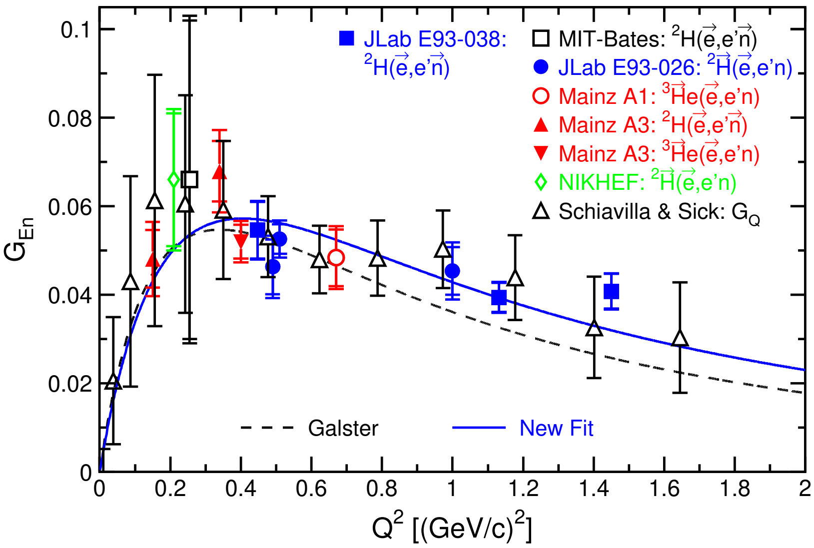

Figure 1: G_E^n versus Q^2. The dashed line reflects the Galster parameterization; the solid line is our modified Galster fit.

We propose to extend measurements of G_E^n to 4.3 (GeV/c)^2. Shown on the Q^2 axis in Fig. 2 is the projected uncertainty for proposed measurement from deuterium at $Q^2 = 4.3$ (GeV/c)^2. Also shown in Fig. 2 are three points [viz., $Q^2 = 1.3$, 2.4, and 3.4 (GeV/c)^2] to be measured in JLab E02-013 from a polarized ^3He target; the error bars here are from the proposal. Displayed in Fig. 2 are measurements made only at JLab.

Polarization measurements of G_E^n at Q^2 above ≈ 1 (GeV/c)^2 require the beam energies available at CEBAF. In the technique demonstrated in E93-038 with a high-luminosity, high-efficiency polarimeter and a dipole magnet ahead of the polarimeter to precess the spin of the neutron, we measured the ratio of two neutron scattering asymmetries: one asymmetry from precessing the neutron polarization vector in a positive direction; the other, from precessing it in a negative direction. In this ratio technique, systematic uncertainties are small because the analyzing power cancels in the ratio, and the beam polarization cancels also because, as demonstrated in E93-038, the beam polarization does not change much during sequential measurements of the scattering asymmetries.

In the high Q^2 region above 1.5 (GeV/c)^2, our present knowledge of the electric and magnetic form factors G_E and G_M for neutrons was obtained from measurements of the angular dependence of the cross section by quasielastic electron-deuteron scattering. Subtraction of the contribution from the proton in the deuteron introduces a large uncertainty. These previous experiments contain large systematic errors because of uncertainties in the theoretical description of the deuteron, mostly from final-state interactions (FSI) and meson-exchange currents (MEC). In the Q^2 region from 1.75 to 4.00 (GeV/c)^2, Lung et al. (1993) reported measurements from SLAC-NE11 of quasielastic $e - d$ cross sections at forward and backward angles which permit a Rosenbluth separation of G_E^n and G_M^n at $Q^2 = 1.75$, 2.50, 3.25, and 4.00 (GeV/c)^2. *Note that the proposed measurement at $Q^2 = 4.3$ (GeV/c)^2 would be the highest value of Q^2 for any G_E^n measurement.* Although Lung et al. (1993) stated that their data from SLAC-NE11 were consistent with $(G_E^n)^2 = 0$ for $1.75 < Q^2$ (GeV/c)$^2 < 4.00$, these data appear consistent also

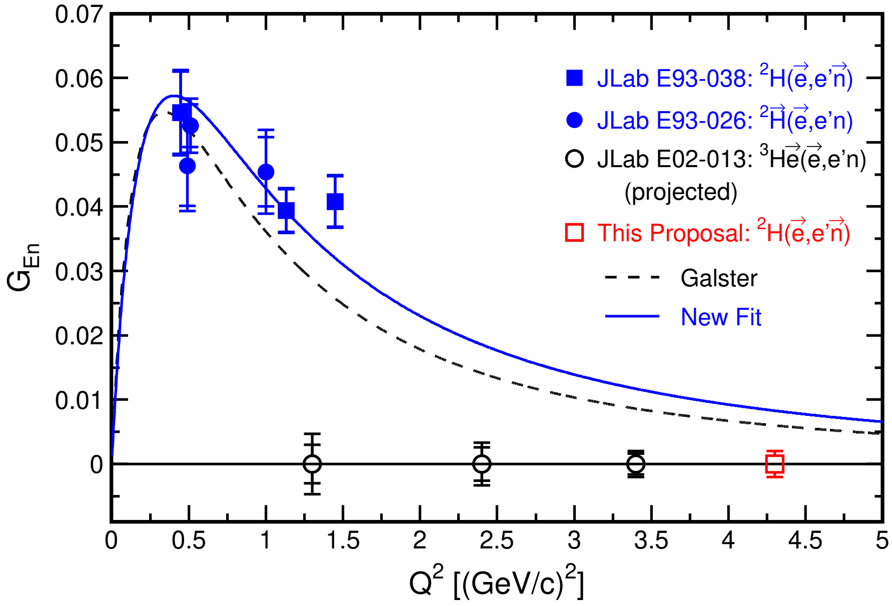

Figure 2: G_E^n versus Q^2. The dashed line reflects the Galster parameterization; the solid line is our modified Galster fit.

with the modified Galster parameterization. The NE11 error bars do not permit distinguishing between $G_E^n = 0$ and the Galster parameterization.

In contrast to the Rosenbluth separation method, the polarization transfer method proposed here permits an experimental determination of the sign of G_E^n. This ability is another nice feature of the polarization transfer technique - especially in view of the fact that nothing is known about the sign of G_E^n at high Q^2. Here we propose to measure G_E^n at $Q^2 = 4.3$ (GeV/c)^2 with sufficient accuracy to challenge rigorous Lattice QCD calculations.

Negele (2000) is leading a major effort to use lattice QCD to understand the structure and interaction of hadrons. Fundamental lattice calculations will become available to solve QCD, the field theory of quarks and gluons. Currently, lattice calculations are limited by computer power; however, increased computing power is becoming available. Lattice QCD calculations are fundamental, whereas various model calculations are not. Lattice QCD has made impressive strides recently, with rigorous methods for separating hard and soft contributions and recent methods for extrapolation to the chiral limit for light quarks using explicit representations of nonanalytic contributions. At the present time, lattice QCD calculations are limited to relatively large quark mass; however, there has been considerable progress in our understanding of how to extrapolate to the chiral limit. Ashley, Leinweber, Thomas, and Young (2004) reported remarkable agreement with the nucleon form factors for Q^2 below 1 (GeV/c)^2. This agreement is remarkable because the result is extrapolated from a light quark mass that is twenty times larger than the physical mass. *Thomas (2003; and Private Communication 2004) indicates that lattice QCD calculations should be able to be made in about two years in the vicinity of $Q^2 = 4$ (GeV/c)^2 and that the extrapolation in this Q^2 region is less stringent because pion loop corrections become suppressed as Q^2 increases.* For $Q^2 < 1$ (GeV/c)^2, the proton electric form factor extrapolation from lattice data match the experimental points; the neutron electric form factor is nearly twice as large as experimental values although it has the correct shape. The neutron electric form factor is very sensitive because it results from a cancellation between the isovector electric form factor G_E^v and the isoscalar electric form factor G_E^s, which yields a relatively small result.

2.2 Better Understanding of Nucleon Structure

Measurements of G_E^n at high Q^2 will help us to understand the symmetry structure of nucleon electromagnetic form factors. Two symmetries play a crucial role: (1) relativistic invariance, which fixes the form of the nucleon current and hence the form of the form factors; and (2) isospin invariance, which gives relations between neutron and proton form factors. While relativistic invariance is expected to be exact, isospin invariance is not exact; however, it is expected to be only slightly broken in a realistic theory of the strong interaction. Isospin invariance leads to the introduction of isoscalar, F_{1S} and F_{2S}, and isovector, F_{1V} and F_{2V}, form factors, and hence to relations among proton and neutron form factors. The observed Sachs form factors, G_E^p and G_E^n, can be obtained from the relations:

$$G_E^p = (F_{1S} + F_{1V}) - \tau\,(F_{2S} + F_{2V}) \tag{2}$$

$$G_E^n = (F_{1S} - F_{1V}) - \tau\,(F_{2S} - F_{2V}) \tag{3}$$

where F_1 and F_2 are the Dirac and Pauli form factors. As a consequence of the two-term structure of Eqs. (2,3), with the second term being multiplied by $-Q^2/4M^2$, G_E^p and G_E^n may have zeros at some value of Q^2, depending on the relative sign of the two terms.

Different models of the nucleon correspond to different assumptions for the Dirac and Pauli form factors. Models with a two-term structure produce results in qualitative agreement with data; for example, a soliton model [Holzwarth (2002)], two relativistic constituent quark models [Miller (2002) and Cardarelli and Simula (2002)], and a model [Lomon (2002)] that couples vector meson dominance with the predictions of pQCD all have this structure and produce results in qualitative agreement with data. Predictions of these models are compared with data in Fig. 3. The chiral soliton model [Holzwarth (2002)] reproduces the dramatic linear decrease observed in $\mu_p G_E^p/G_M^p$ for $1 < Q^2 < 6$ (GeV/c)^2; however, this model fails to reproduce the neutron data at large Q^2. A light-front calculation using pointlike constituent quarks surrounded by a cloud of pions [Miller(2002)], denoted "LFCBM", describes the neutron data, but falls below the proton data at high Q^2. A one-gluon exchange light-front calculation, denoted "OGE CQM", using constituent quark form factors fitted to $Q^2 < 1$ (GeV/c)^2 data [Cardarelli and Simula (2000)] agrees with the neutron data, but deviates from the proton data above $Q^2 \sim 3.0$ (GeV/c)^2. The Lomon model, denoted "VMD + pQCD", agrees with the proton data but falls below the neutron data above $Q^2 \sim 1.2$ (GeV/c)^2.

In 1973, Iachello, Jackson, and Lande [1973] suggested that the structure of the nucleon consists of two components: (1) an intrinsic structure (presumably three valence quarks), and (2) a meson cloud parameterized in terms of vector mesons (ρ, ω, ϕ). In this 1973 model of the nucleon, the external photon couples to both the intrinsic structure and the meson cloud. Iachello [2003] showed that the 1973 model agrees well with the new Hall A data on the proton form factor ratio $\mu_p G_E^p/G_M^p$; however, this 1973 model disagrees with the JLab E93-038 data on the neutron form factor ratio $\mu_n G_E^n/G_M^n$. Recently, Bijker and Iachello [2004] carried out a new isospin-invariant calculation that yielded agreement with the E93-038 neutron data. This 2004 calculation allows an intrinsic spin-flip amplitude, in addition to the spin-flip amplitude coming from the vector mesons. The results from both the 1973 and 2004 calculations are shown in Fig. 4 as a function of Q^2; the ratio for protons (neutrons) is shown in the top (bottom) panel. For G_E^p, the 1973 calculation predicts a zero at about 8 (GeV/c)^2, whereas the 2004 calculation

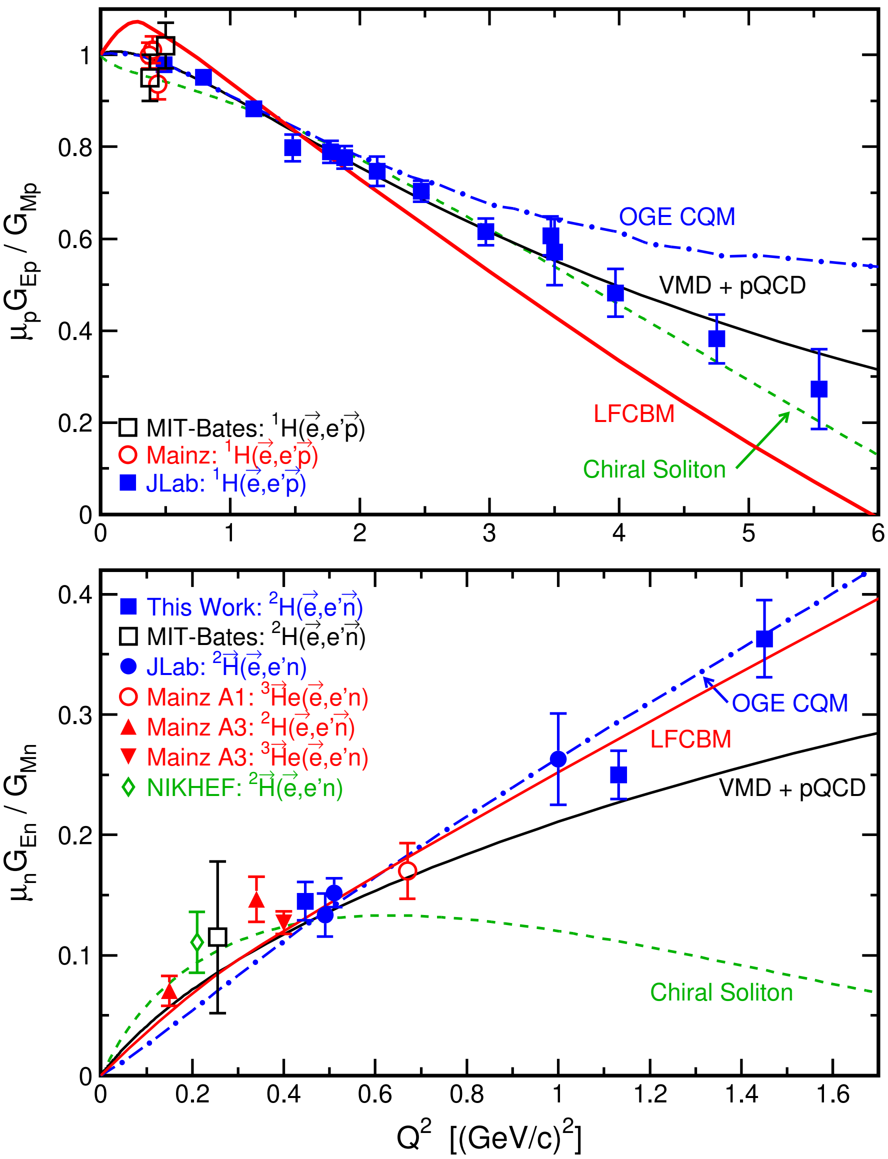

Figure 3: Predictions of selected models (see text for descriptions and the legend) for $\mu_p G_E^p / G_M^p$ and $\mu_n G_E^n / G_M^n$ compared with proton and neutron data. The neutron data symbols are the same as in Fig. 1.

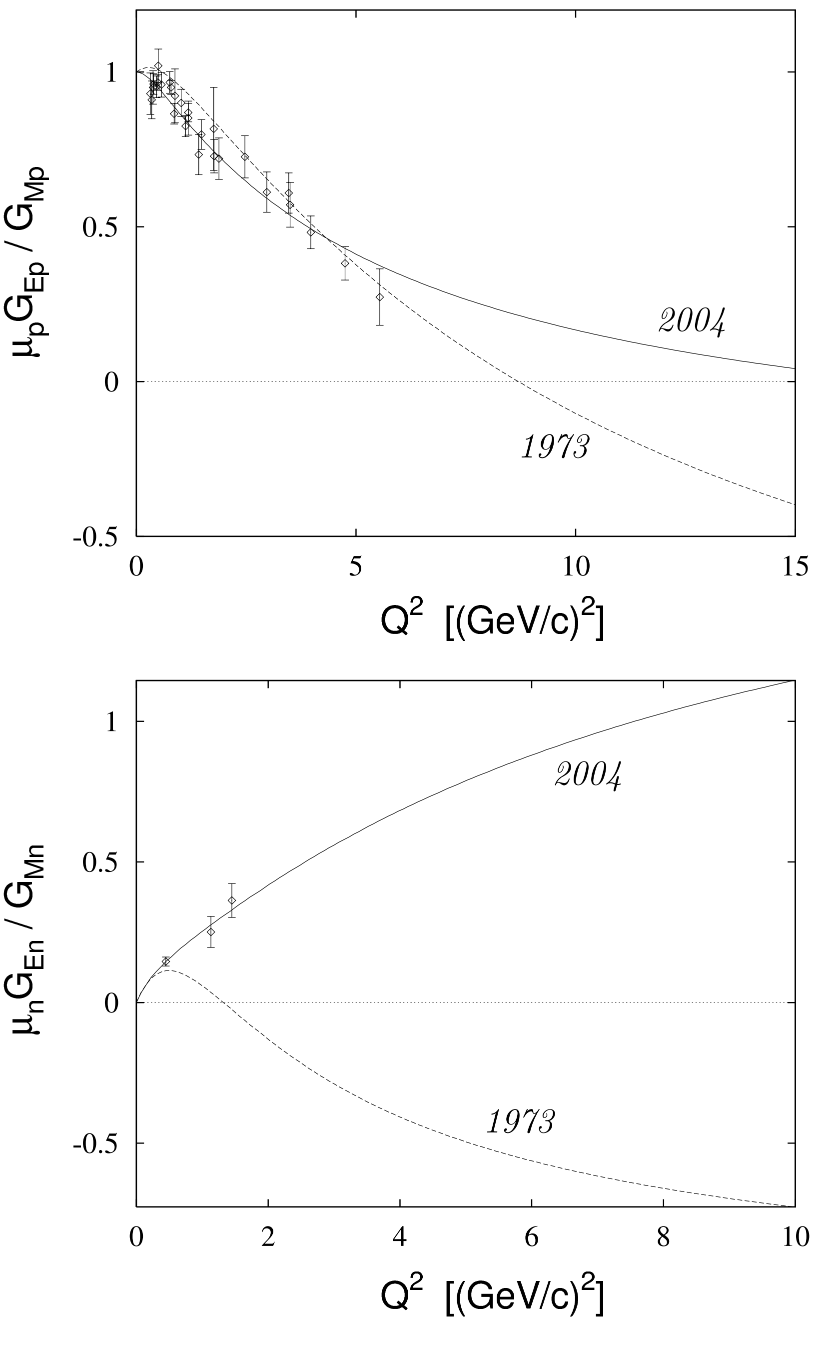

Figure 4: Predictions of the 1973 model (dashed) by Iachello, Jackson, and Lande, and the 2004 model (solid) by Bijker and Iachello for $\mu_p G_E^p / G_M^p$ (top panel) and $\mu_n G_E^n / G_M^n$ (bottom panel) compared with proton and neutron data.

pushes this zero to about 15 (GeV/c)^2; for G_E^n, the 2004 calculation predicts a zero at Q^2 in excess of 20 (GeV/c)^2. To discriminate between various models, it is necessary to determine the Q^2 values where the zero crossings occur. The two calculations shown in Fig. 4 represent two limiting cases:

(1) 1973 calculation: Helicity here is strictly conserved in the intrinsic part and the Pauli form factor F_2 comes entirely from coupling to the vector mesons.

(2) 2004 calculation: Helicity flip is allowed in the intrinsic part (as in the light front calculations). The anomalous part of the form factor, F_2, comes almost entirely from intrinsic spin-flip components (not from vector mesons).

The 2004 calculation is consistently better for the proton data except at the highest Q^2 point. The neutron data need the 2004 calculation; the 1973 calculation deviates markedly from the E93-038 neutron data. Measurements of the sign of G_E^p and G_E^n are crucial for disentangling the structure of the nucleon.

2.3 Better Understanding of Effects of Relativistic Quarks

A motivation for measuring G_E^n at higher Q^2 is to obtain a better understanding of effects of relativistic quarks. In the Light Front Cloudy Bag Model (LFCBM) of Miller (2002), the nucleon is modeled as a relativistic system of three bound constituent quarks immersed in a cloud of pions. The pionic cloud is important for understanding low-momentum transfer physics, whereas the quarks dominate at high values of Q^2. The LFCBM predicts that the contribution to G_E^n from the relativistic quarks exceeds the Galster parameterization, as shown in Fig. 5 (top panel); and that the relativistic quarks make the main contribution to G_E^n at high Q^2, as shown in Fig. 5 (bottom panel).

2.4 Better Understanding of Electron Scattering Data From Nuclei

In their paper on electron scattering from nuclei, Drechsel and Giannini (1989) state (on page 1109) that *"All calculations of nuclear electromagnetic properties suffer from the poor knowledge of G_E^n."* As Q^2 increases, the values of G_E^p, the electric form factor of the proton, approach the values of G_E^n, represented by the modified Galster parameterization. Plotted in Fig. 6 (top panel) as a function of Q^2 are the neutron electric form factor for the modified Galster parameterization, and the proton electric form factor points measured in JLab E93-027 and E99-007. The measured G_E^p points have been fitted with the following parameterization:

$$G_E^p = G_D\,[1 - 0.14(Q^2 - 0.30)] \qquad (\mathit{Fit\ to\ Hall\ A\ FPP\ Measurements}) \tag{4}$$

with

$$G_D \;\equiv\; (1 + Q^2/0.71)^{-2} \qquad (\mathit{Dipole}) \tag{5}$$

The magnitude of G_E^n is not insignificant compared to G_E^p in the Q^2 region above about 2 (GeV/c)^2. The value of G_E^n from the modified Galster fit exceeds the value of G_E^p above $Q^2 \sim$ 4.4 (GeV/c)^2; accordingly, the isovector electric form factor would become negative in this Q^2 region. As shown in Fig. 6, the most recent model of Bijker and Iachello (2004) predicts that the isovector electric form factor becomes negative at a Q^2 of about 3 (GeV/c)^2; whereas the model of Miller et al. (2002) predicts a crossover at $\sim$4.3 (GeV/c)^2. The isovector form factor

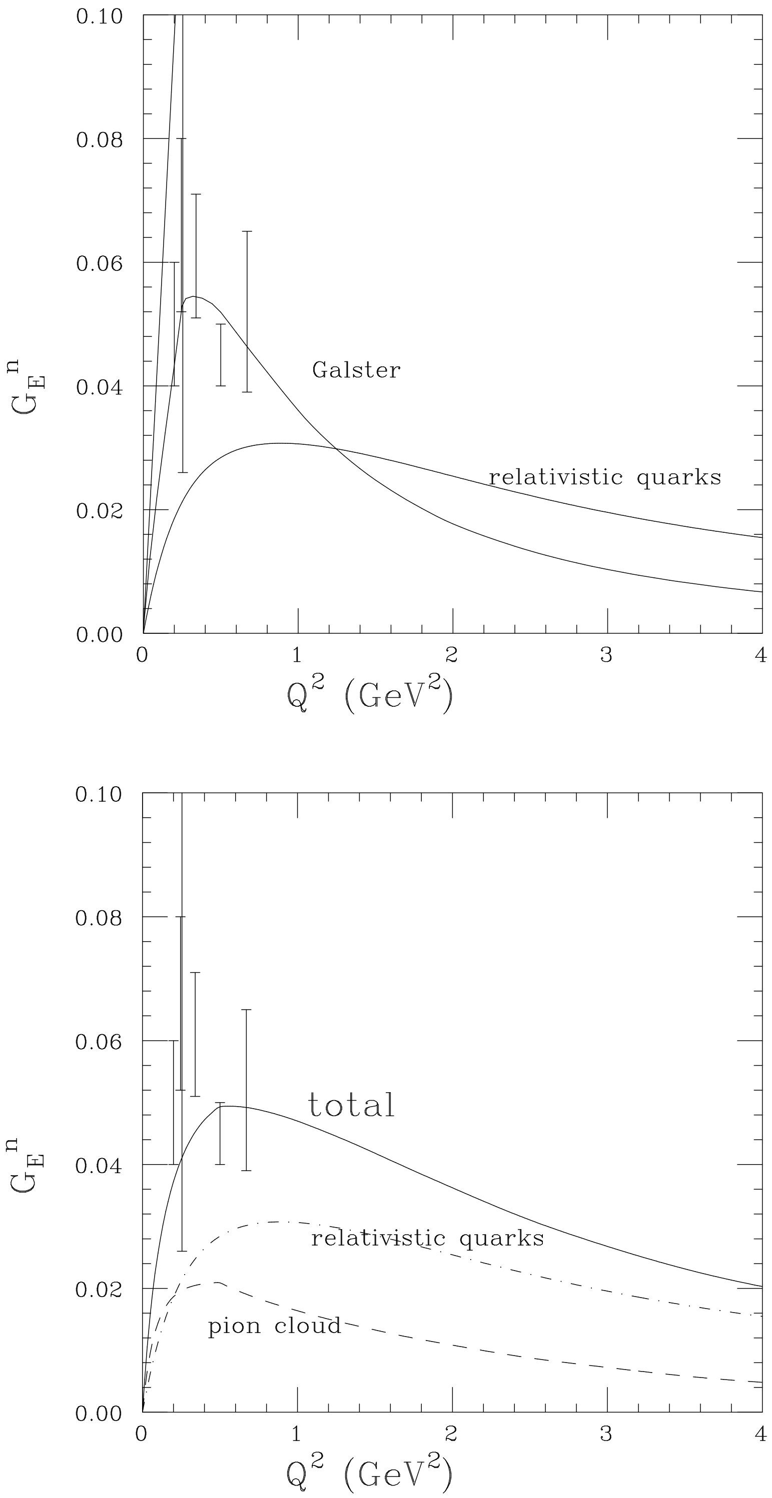

Figure 5: Calculation of G_E^n by Miller (2002): relativistic quarks contribution (top panel) and total LFCBM calculation (bottom panel). [Figure taken from Miller (2002).]

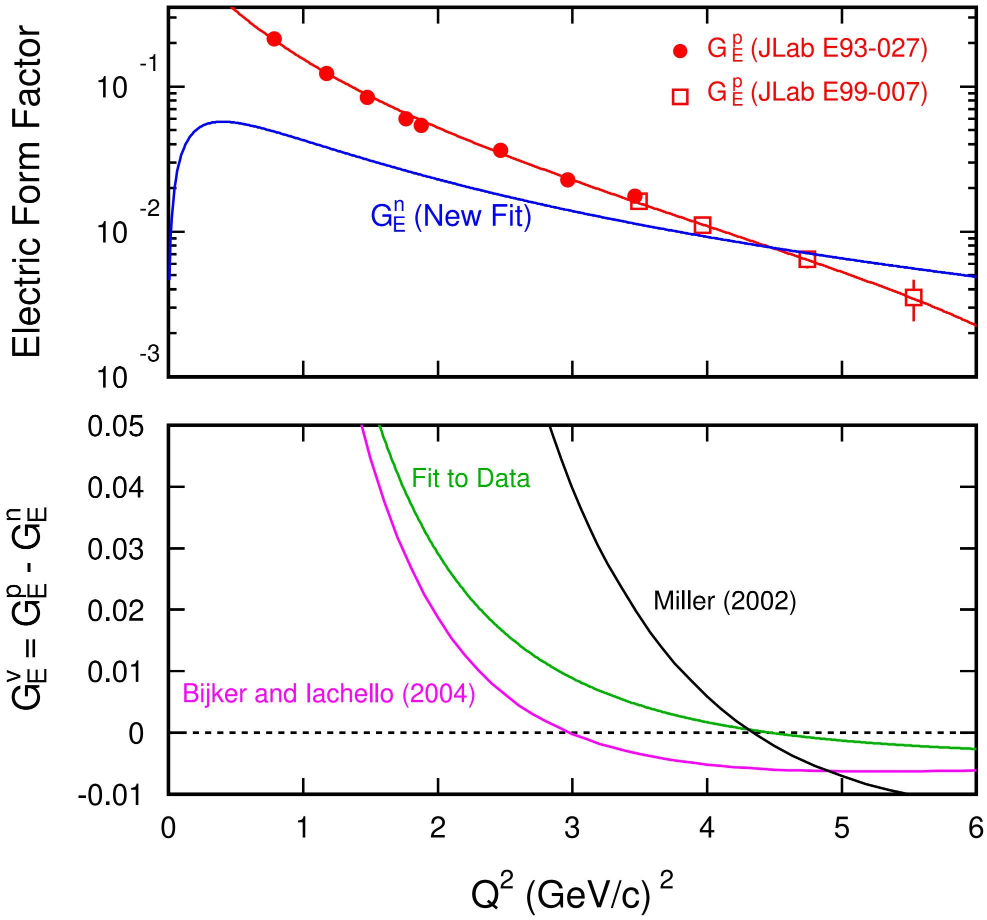

Figure 6: Proton, neutron, and isovector form factors as a function of Q^2. The red solid line in the top panel is a parameterization from Eq. (4) for G_E^p. Bottom panel: the green line is a difference of the G_E^p and G_E^n parameterizations from the top panel, the magenta line is a calculation by Bijker and Iachello (2004), and the black line is a calculation by Miller et al. (2002).

[i.e., a difference between G_E^p (E93-027/E99-007) and G_E^n (New Fit from E93-038)] is plotted in the bottom panel of Fig. 6. The G_E^p data measured in E93-027 turned out to be a surprise — falling faster with Q^2 than expected from the global analysis of earlier SLAC data. The nature of the decrease of G_E^n with Q^2 may be a surprise also.

Because the isovector electric form factors of nuclei are proportional to the difference $G_E^p - G_E^n$ (and the isoscalar electric form factors are proportional to the sum $G_E^p + G_E^n$), the value of G_E^n is needed for the understanding of electron scattering experiments that probe electric structure functions at high momentum transfer. The ratio of the isoscalar cross section to the isovector cross section depends sensitively on the value of G_E^n:

$$\frac{\sigma_{isoscalar}}{\sigma_{isovector}} = \left(\frac{G_E^p + G_E^n}{G_E^p - G_E^n}\right)^2 \tag{6}$$

This ratio is plotted in Fig. 7 as a function of Q^2. This ratio is unity if $G_E^n = 0$; however, this ratio is about 900 at $Q^2 = 4.3$ (GeV/c)^2 if G_E^n continues to follow the modified Galster parameterization and if G_E^p follows Eq. (4). A better knowledge of G_E^n is needed for the interpretation

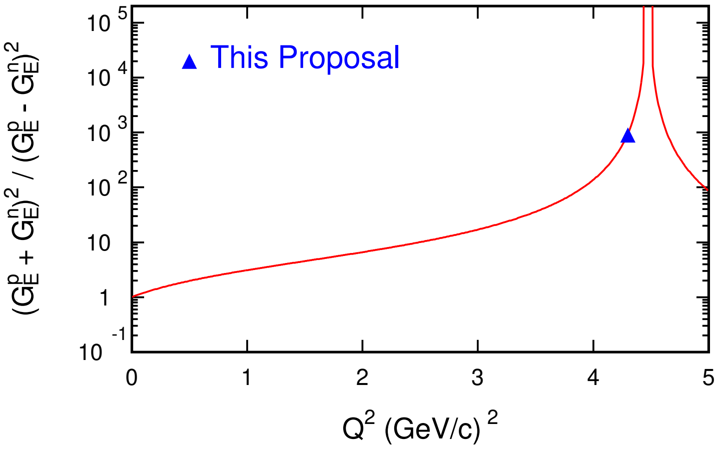

Figure 7: The ratio of isoscalar and isovector cross-sections [Eq. (6)] as a function of Q^2. We assume the modified Galster parameterization (New Fit from E93-038) for G_E^n and the parameterization from Eq. (4) for G_E^p.

of electron scattering from nuclei at high momentum transfer. This knowledge is needed for the analysis of few-body data from measurements at Jefferson Lab, which are in the Q^2 range above the existing G_E^n data. With an uncertainty $\Delta G_E^n \approx 0.0020$, we will be able to distinguish easily between $G_E^n = 0$ and the modified Galster parameterization at the Q^2 values proposed herein.

2.5 Nuclear Physics Corrections and Reaction Mechanism Questions

Figure 8 shows the results from E93-038 for three cases: (1) The black triangles are for a point acceptance; (2) the red circles are acceptance-averaged PWBA values; and (3) the blue squares are the acceptance-averaged values based on Arenhoevel's full calculation [including FSI, MEC, and IC]. In E93-038, the nuclear physics corrections [for FSI, MEC, and IC] increased G_E^n over the values obtained with the PWBA by 5.6, 4.0, and 3.3 percent at $Q^2 = 0.45$, 1.13, and 1.45 (GeV/c)^2, respectively. While the magnitude of the nuclear corrections are expected to continue to decrease with increasing Q^2, the nuclear corrections are more reliable [and most likely smaller] for deuterium than for helium. Arenhoevel [2003] carried out calculations for deuterium for the proposed kinematics at $Q^2 = 4.3$ (GeV/c)^2; his results are shown in Fig. 9.

Also, the reaction mechanism is expected to be simpler in deuterium than in helium. In the case of the proton form factor, reaction mechanism questions remain when comparing the Rosenbluth separation measurements with the recoil polarization measurements. Two or more independent measurements of the neutron are needed to alleviate questions about the reaction mechanism.

3 Theoretical Background

Arenhoevel (1987) calculated the effect of the electric form factor of the neutron on the polarization transfer in the $d(\vec{e}, e'\vec{n})p$ reaction in the quasifree region, where the deuteron serves as a neutron target while the proton acts mainly as a spectator. Using a nonrelativistic theory and a realistic nucleon-nucleon potential, Arenhoevel found that the sideways polarization of the recoil neutron $P_{S'}$, which vanishes for coplanar kinematics and unpolarized electrons, is most sensitive

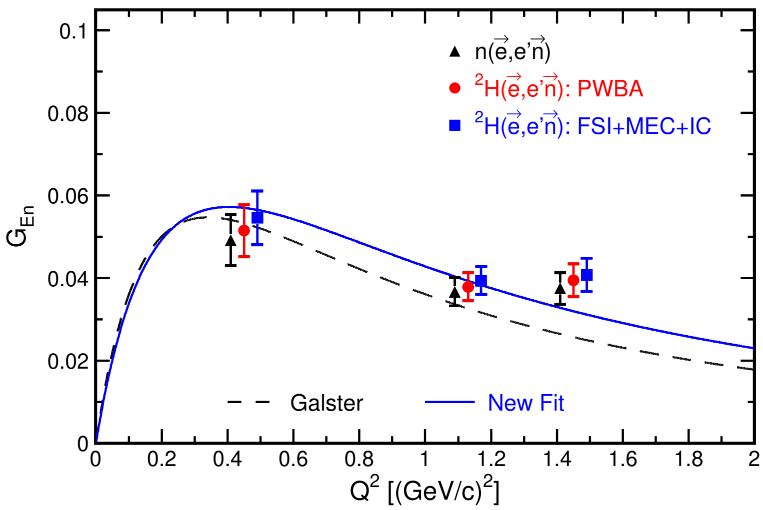

Figure 8: Comparison of the final results for G_E^n extracted from analyses assuming $n(\vec{e}, e'\vec{n})$ elastic scattering and a point acceptance (black triangles), the acceptance-averaged $^2\mathrm{H}(\vec{e}, e'\vec{n})^1\mathrm{H}$ Arenhövel PWBA model (red circles), and the acceptance-averaged $^2\mathrm{H}(\vec{e}, e'\vec{n})^1\mathrm{H}$ Arenhövel FSI+MEC+IC model (blue squares). The error bars shown are the quadrature sum of the statistical and systematic errors.

to G_E^n for neutron emission along the momentum-transfer direction in the quasifree case. Using the parameterization of Galster et al. (1971) for G_E^n, Arenhoevel's calculation indicates that even away from the forward-emission direction (with respect to the direction of the momentum transfer $\vec{q}$), the increase in the sideways polarization of the neutron $P_{S'}$ is small for $G_E^n = 0$, but increases when G_E^n is switched on, and that this increase prevails up to a neutron angle of nearly 30^o measured with respect to $\vec{q}^{\,c.m.}$ in the center-of-mass system. In the forward direction with respect to $\vec{q}^{\,c.m.}$, Arenhoevel found also that the neutron polarization $P_{S'}$ is insensitive to the influence of final-state interactions (FSI), meson-exchange currents, and isobar configurations, and that this lack of sensitivity holds again up to an angle of nearly 20^o away from the forward direction with respect to $\vec{q}^{\,c.m.}$, which corresponds to a laboratory angle of about a few degrees away from the forward direction with respect to the $\vec{q}^{\,lab}$. Arenhoevel also studied the influence of different deuteron wave functions on the sideways neutron polarization $P_{S'}$. His results for quasifree kinematics (i.e., for neutron emission along $\vec{q}$) show almost no dependence on the deuteron model. The Arenhoevel calculation shows that dynamical uncertainties are very small. Finally, Beck and Arenhoevel (1992) investigated the role of relativistic effects in electrodisintegration of the deuteron for quasifree kinematics. They found that the dependence on the parameterization of the nucleon current in terms of Dirac-Pauli or Sachs form factors is reduced considerably by inclusion of the relativistic contributions. Also, for quasifree emission, Arenhoevel (2002) demonstrated that $P_{L'}$ is insensitive to FSI, MEC, IC, and to theoretical models of deuteron structure.

Rekalo, Gakh, and Rekalo (1989) used the relativistic impulse approximation to describe the polarization effects sensitive to G_E^n in deuteron electrodisintegration. In the deuteron quasielastic peak, the neutron polarizations calculated in the relativistic approach agree with the results of Arenhoevel (1987). A later study by Mosconi, Pauschenwein, and Ricci (1991) of nucleonic and pionic relativistic corrections in deuteron electrodisintegration does not change the results of Arenhoevel. Laget (1990) investigated the effects of nucleon rescatterings and meson-exchange currents on the determination of the neutron electric form factor in the $d(\vec{e}, e'\vec{n})p$ reaction. He

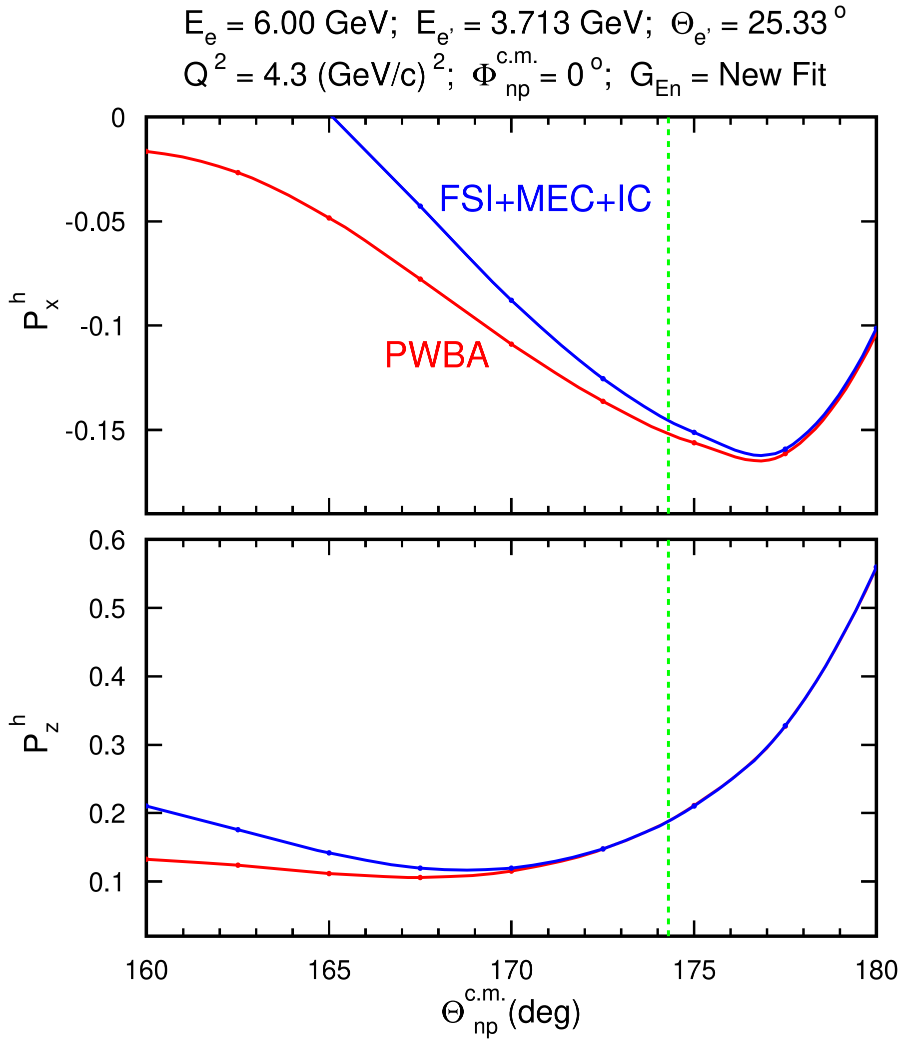

Figure 9: Comparison of Arenhoevel's PWBA and FSI+MEC+IC calculations of P_x^h and P_z^h at $Q^2 = 4.3$ (GeV/c)^2.

concluded that the measurements of the sideways polarization of the neutron appears to be the most direct way to determine the neutron electric form factor. He concluded also that in quasifree (colinear) kinematics, the neutron polarization in the exclusive reaction is equal to the value expected in the elementary reaction $n(\vec{e}, e')\vec{n}$ and that corrections from final-state interactions and meson-exchange currents are negligible above $Q^2 = 0.30$ (GeV/c)^2, but that these corrections become sizeable below this momentum transfer; however, Herberg et al. (1999) found that (even in the quasifree peak) corrections for FSI in $d(\vec{e}, e'\vec{n})p$ measurements at Mainz amounted to (8±3)% for $Q^2 = 0.34$ (GeV/c)^2 and (65±3)% for $Q^2 = 0.15$ (GeV/c)^2 of the value unperturbed by FSI. In E93-038, we found that the nuclear physics [FSI+MEC+IC] corrections were small and decreased with increasing Q^2. The nuclear physics corrections increased G_E^n over the value obtained with the PWBA by only 5.6, 4.0, and 3.3 percent at $Q^2 = 0.45$, 1.13, and 1.45 (GeV/c)^2, respectively. These corrections were based on the model of Arenhoevel et al. (1988).

4 Description of the Experiment

4.1 Experimental Arrangement

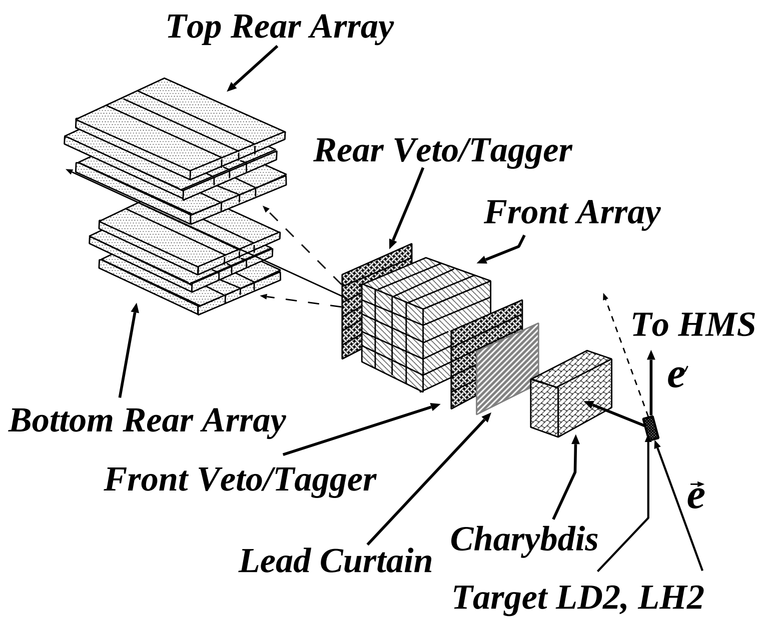

Figure 10: Schematic diagram of the experimental arrangement in E93-038.

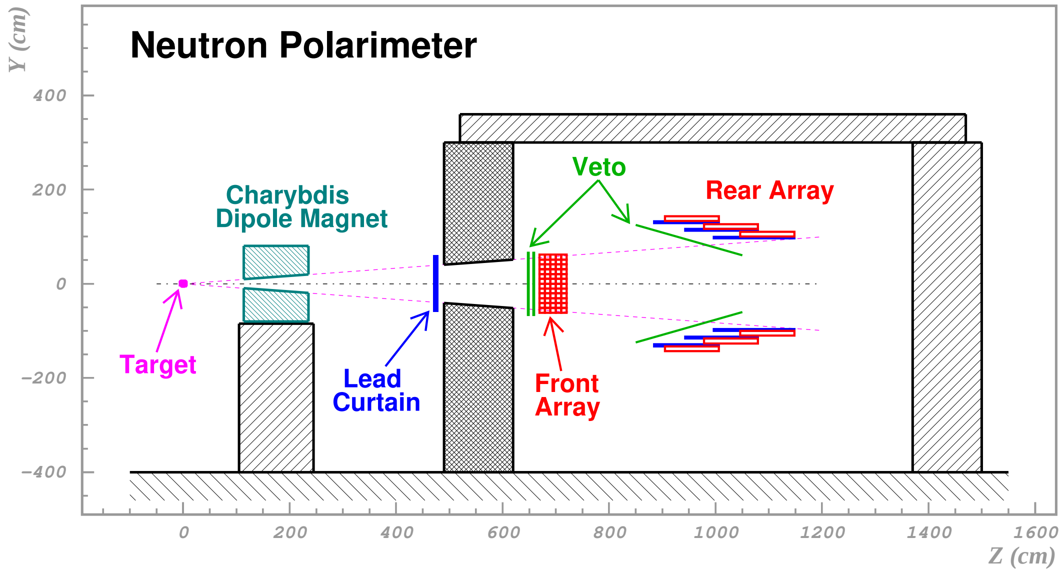

Figure 11: Neutron polarimeter to be used in the measurements.

The experimental arrangement is similar in principle to the one used in E93-038 (shown in Fig. 10). A polarimeter detects the recoil neutron from the quasielastic d($\vec{e}$,e'$\vec{n}$)p reaction and measures the up-down scattering asymmetry from the projection of the polarization vector on the transverse axis. A dipole magnet (CHARYBDIS) in front of the polarimeter precesses the neutron polarization vector through an angle χ to permit measuring the scattering asymmetry

ξ_+ from the polarization vector component on the transverse (or sideways) direction. With another measurement of the scattering asymmetry ξ_- for a precession through an angle $-\chi$, the ratio of G_E and G_M is given by

$$g \equiv \left(\frac{G_E}{G_M}\right) = K_R\, tan(\chi)\, \frac{(\eta+1)}{(\eta-1)} \tag{7}$$

where the asymmetry ratio

$$\eta \equiv \frac{\xi_-}{\xi_+} = \frac{P^x_-}{P^x_+} \tag{8}$$

and K_R is a kinematic function that is determined by the electron scattering angle θ_e in the d($\vec{e}$,e'$\vec{n}$)p reaction. For a total data-acquisition time T, the time fractions for measuring ξ_+ and ξ_- are optimized to minimize the statistical uncertainty in g. The scattered electron from the d($\vec{e}$,e'$\vec{n}$)p reaction is detected with the high-momentum spectrometer (HMS) in coincidence with the recoil neutron.

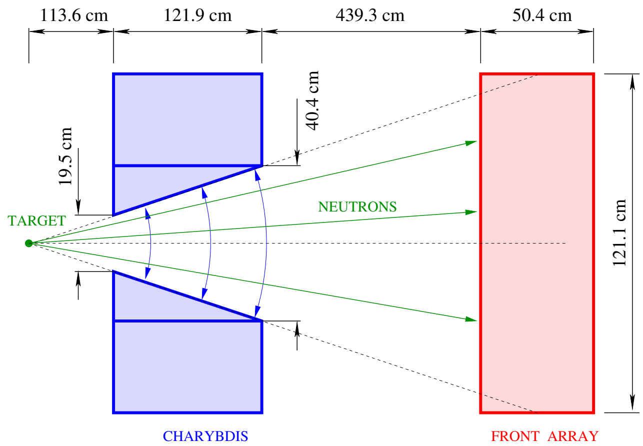

Figure 12: Tapered poles of Charybdis (side view). [Drawing is not to scale to emphasize the vertical dimension.]

The polarimeter to be used for these measurements (see Fig. 11) is an enhanced version of the one used for E93-038. In order to increase the vertical acceptance of the front array, we plan to increase the number of detectors in each layer from 5 to 12. In order to increase the efficiency, we are increasing the number of detector layers in the front array to five layers [from the four used in E93-038], and we are inserting 3-cm steel converters ahead of each layer in the rear detector arrays. The thickness of the converters was optimized to maximize the gain (∼1.6) in the detection efficiency for neutrons [Semenova et al. (2002)]. Other advantage of using the converters is that the converters ahead of the each detector in the rear array will prevent the detection of the gammas from the π^0 decays in the front array. Examination of the geometry of the enhanced polarimeter in Fig. 11 reveals that the mean photon path length through the center of the middle-layer converter is 10.6 cm [= ∼6.0 radiation lengths]; similarly, the mean path length is 6.5 [∼5.5] radiation lengths for the outer [inner] converter. Note that a thickness of 5.5 radiation lengths reduces the energy of the incident photon to ∼0.40% of its initial value. We optimize the geometry so that the mean scattering angle is at the peak of the analyzing power. The polarimeter now consists of 60 detectors in the front array and 18 detectors in each of two rear arrays for a total of 96 detectors. A double layer of veto/tagger detectors is located ahead of the front array, and a tagger detector is located in front of the upper and

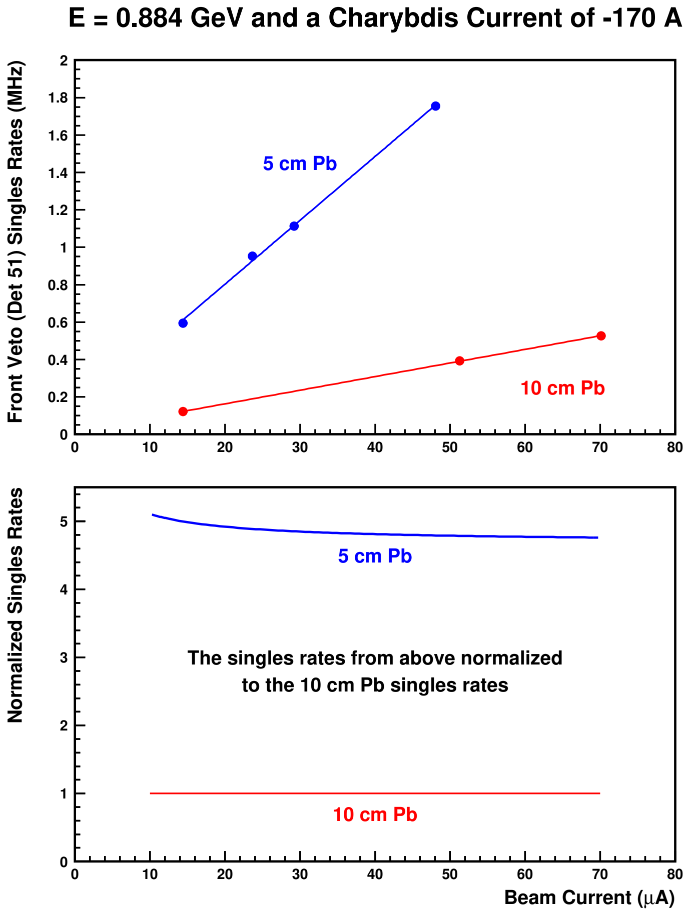

Figure 13: Singles rates for beam energy of 884 MeV and a CHARYBDIS current of -170 A.

lower rear arrays. The proposed configuration of the rear tagger decreases the single rates in the tagger from the charged background and simplifies the identification of neutrons in the rear array (compared with E93-038). To permit high luminosity, the dimensions of each of the 60 detectors in the front array are 10 cm×10 cm×100 cm, and the 18 [10 in×40 in×4 in] detectors in each rear array are shielded from the direct path of neutrons from the target.

A significant advantage of this technique for measuring the ratio of the two scattering asymmetries is that the scale and systematic uncertainties are minimal because the relative uncertainty in the analyzing power of the polarimeter does not enter in the ratio. The same is true for the beam polarization P_L because, as demonstrated in E93-038, P_L does not change much during sequential measurements of ξ_+ and ξ_-.

In the cross-ratio method of analysis of the scattering asymmetries measured in the polarimeter, Ohlsen and Keaton (1973) showed that false asymmetries cancel to all orders from helicity-dependent errors in charge integration or system dead-times, or from errors in detection efficiency and acceptances; and that false asymmetries cancel to first order from misalignments with respect to $\vec{q}$, or from a difference in the beam polarization for the two helicity states. The cross ratio is the ratio of two geometric means $(N_U^+ N_D^-)^{1/2}$ and $(N_U^- N_D^+)^{1/2}$, where $N_U^+(N_D^-)$ is the yield in the peak for scattering neutrons up (down) when the helicity is positive (negative).

The systematic and scale uncertainties achieved in E93-038 are listed in Table I of Appendix A. The overall systematic uncertainties are of the order of 2%.

In E93-038, we used the CHARYBDIS dipole magnet with an 8.25-inch gap and 2-inch field clamps. The 8.25-inch gap was large enough to illuminate fully the 0.5-m high by 1-m wide front array of the E93-038 polarimeter. To illuminate fully the increased front array of the proposed polarimeter, the tapered gap between the magnet poles (19.5 cm at the entrance and 40.4 cm at the exit of the magnet, see Fig. 12) is chosen. Such a configuration of the gap permits minimizing the current in the magnet that is needed to reach the desired field integral. Other advantages of such a gap are:

1. The magnetic field in the gap is almost perpendicular to the momentum of all neutrons emitted from the target in to the front array;

2. The Charybdis poles provide additional collimation to protect the polarimeter rear array from the direct particles from the target.

The precession angle χ is the angle of rotation of the polarization vector after traversing the magnetic field. The neutron spin precession angle χ is given by

$$\chi \;=\; -\frac{ge}{2M_pc\beta_n}\int B\Delta l \;=\; \frac{1.913e}{M_pc\beta_n}\int B\Delta l \tag{9}$$

where $g/2 =$ -1.913. The maximum central $\int B\Delta l = 2.39$ Tm for CHARYBDIS with an 8.25-inch gap.

The 15-cm lead curtain ahead of the polarimeter is required to attenuate electromagnetic radiation and also to reduce the flux of charged particles incident on the polarimeter. The curtain thickness is chosen to maintain an acceptable singles rate at a beam current of 100 μA (see description of the simulation in Section 4.5). *If we find during the experiment that the single rates in the front array are too high, we will increase the thickness of the lead curtain; the loss in the neutron rate will be compensated partly with a smaller fraction of corrupted events.* In E93-038, the singles counting rate in one of the detectors decreases markedly when the thickness of the Pb increases from 5 cm to 10 cm; for example, the singles rates in one of the veto detectors (160 cm wide $\times$ 11 cm high $\times$ 0.64 cm thick) at a distance of about 6.7 m from a 15-cm LD_2 target are plotted in Fig. 13 as a function of the electron beam current at an energy of 884 MeV. For all beam currents, the singles rate is about five times higher with a 5-cm Pb curtain. E93-038 used a 10-cm lead curtain in order to run at higher beam currents. We do not have data with a 5-cm lead curtain at higher beam energies. E93-038 ran with a 10-cm Pb curtain for all these energies.

To measure the false asymmetry or the dilution of the asymmetry from the two-step process $d(\vec{e}, e'\vec{p})n + Pb(\vec{p}, \vec{n})$ we acquire data with an LH_2 target. In the second charge-exchange step, the sign of the polarization transferred to the neutron will be opposite to that from the primary $d(\vec{e}, e'\vec{n})p$ process because the sign of the magnetic moment of the proton is opposite that of the neutron. This effect increases as the $p - n$ charge exchange cross section increases in going to low Q^2.

4.2 Kinematics

Table 1 lists the kinematic conditions and the $B\Delta l$ required to precess the neutron polarization vector through χ degrees. The accelerator should be able to deliver a beam polarization of 80% at any energy (see Fig. 26). The range of reasonable angles of neutron spin precession is limited on the small-angle side by the requirement to have the magnetic field in CHARYBDIS strong enough to deflect a significant part of the quasielastic protons away from the front array of the

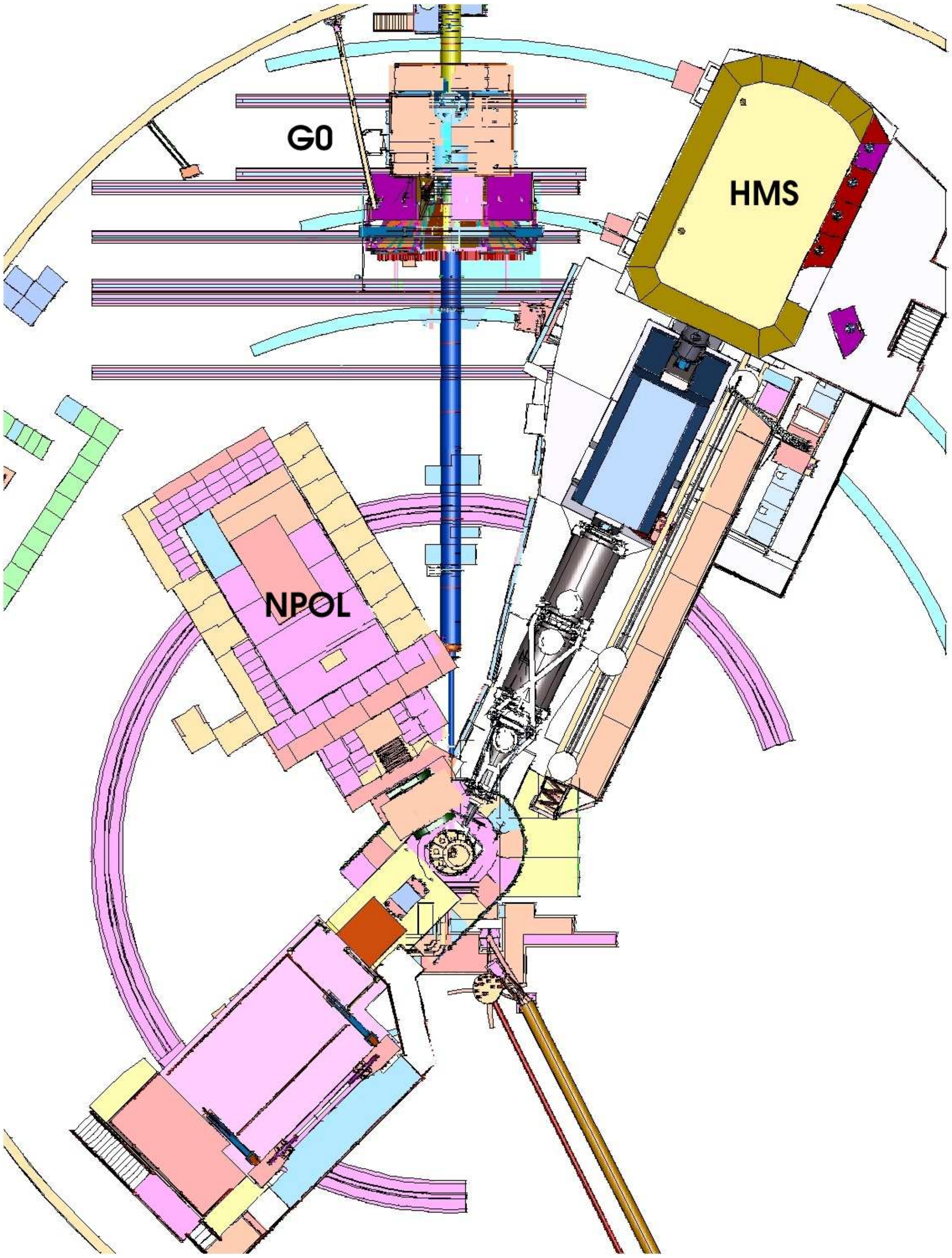

Figure 14: Footprint in Hall C of the polarimeter shielding enclosure for a neutron angle of 31.0 degrees and a mean flight path of 7.0 m. The shielding enclosure is compartible with the setup for G_0 experiment.

Four-Momentum Transfer, Q^2 $(\mathrm{GeV}/c)^2$	4.3
Beam Energy, E_0 (GeV)	6.00
Electron Scattering Angle, θ_e (deg)	25.33
Scattered Electron Momentum, $P_e^{;}$ (GeV/c)	3.713
Neutron Scattering Angle, θ_n (deg)	31.0
Neutron Momentum, P_n (GeV/c)	3.084
Neutron Kinetic Energy, T_n (GeV)	2.285
Flight Path, x (m)	7.0
Precession Angle, χ (deg)	25
Field Integral to Precess Neutron Spin through χ Degree, $B\Delta l$ (Tm)	0.6830

Table 1: Kinematic conditions at a neutron scattering angle of 31.0^o. Also listed is the Charybdis field integral $B\Delta l$ required to precess the neutron polarization vector.

polarimeter, and on the large-angle side by the fact that the statistical uncertainty increases with precession angle χ, as shown in Fig. 19. A precession angle χ of 25 deg. was chosen for Q^2 = 4.3 (GeV/c)^2. Smaller precession angles were avoided because the smaller Charybdis current would reduce the deflection of protons away from the front array.

4.3 Footprint in Hall C

Figure 14 is a footprint in Hall C of the NPOL and the HMS. The The apparatus for the G_0 experiment in the back-angle configuration is shown also. The proposed G_E^n apparatus is compatible with the G_0 setup in the back-angle configuration.

4.4 Count Rates

The rate of electron-neutron coincidence events, which comes from quasielastic scattering of electrons on the 15-cm LD_2 target, was projected at $Q^2 = 4.3$ (GeV/c)^2 for a beam current of 100 μA (which corresponds to a beam luminosity $L = 4.77 \times 10^{38}$ cm^{-2}s^{-1}). The calculation was done for a momentum bite $\Delta p/p$ of $-3/+10\%$ for the scattered electron. This HMS momentum bite (combined with the cuts on the missing momentum and HMS-NPOL coincidence time) helps to suppress the neutrons associated with pion production (see Figs. 15, 20).

The acceptances for E93-038 were calculated for the HMS in the normal-quad mode and in the rear position. We used the kinematic conditions from Table 1 for $Q^2 = 4.3$ (GeV/c)^2. Based on the acceptance-averaged HMS-NPOL coincidence rate of quasielastic events, $< R_{MCEEP} >$, from MCEEP [Ulmer (1991) version 3.6 includes radiative corrections], we estimated the real-event rate R_{real} for an HMS efficiency $\epsilon_{HMS} = 0.92$ [which is the product of a single-hit fraction in the wire chambers (0.95) and an efficiency for tracking a good electron (0.97)], the HMS momentum bite of -3/+10%, and the HMS-NPOL coincidence time-of-flight ($cTOF$) window of ± 1 ns. For this estimation, we simulated the neutron polarimeter efficiency, ϵ_n, (including neutron transmission through 15-cm lead curtain and lost of events due to analysis cuts) and the polarimeter analyzing power, A_Y, with the FLUKA 2002 code (see also Section 5 and Fig. 25). Listed in column 2 (3) of Table 2 are neutron polarimeter and HMS (HRS) acceptances, estimated neutron polarimeter parameters (viz., A_Y and ϵ_n), and the calculated real event rate

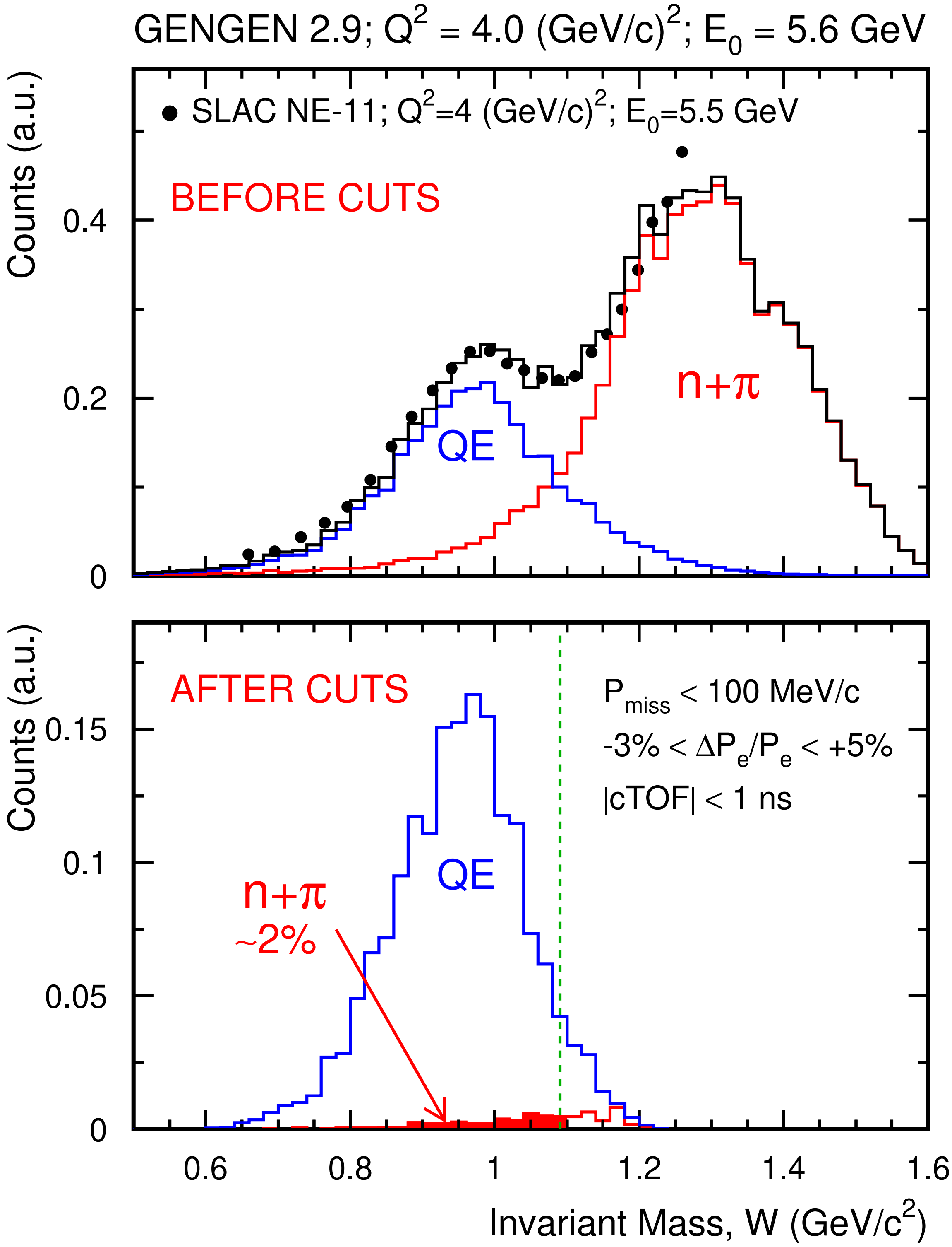

Figure 15: Invariant mass spectra before (top panel) and after (bottom panel) cuts on the scattered electron momentum, the missing momentum, and an HMS-NPOL coincidence time-of-flight. Quasielastic and pion-production spectra are simulated separately with GENGEN 2.9 code [Kelly (2000)] and normalized on the invariant mass spectrum at similar kinematics from SLAC NE-11 (Lung et al. (1993)].

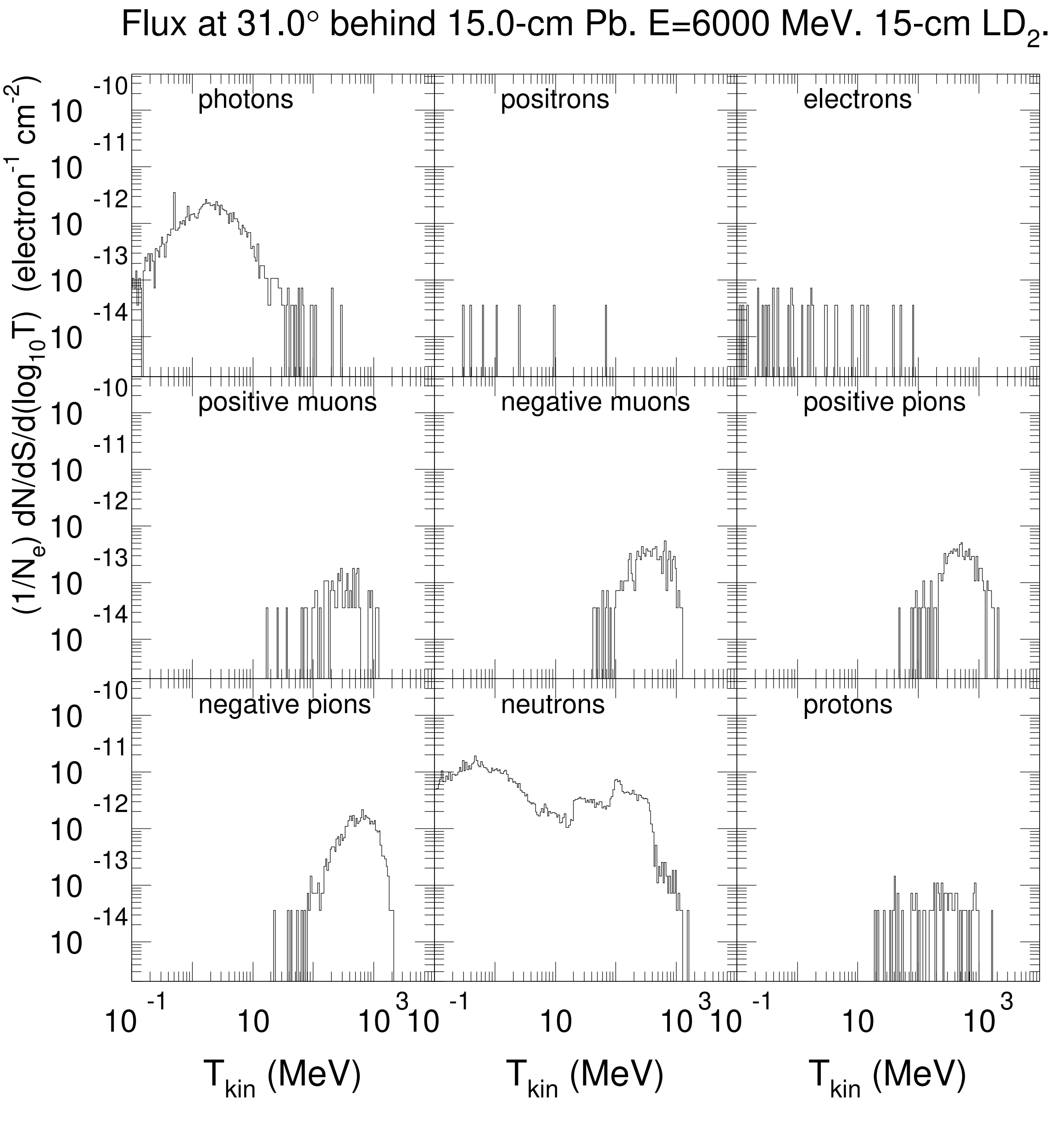

Figure 16: Simulated spectra of the particles at 31.0^o behind 4-in Pb curtain from 6.00 GeV electron beam incident on a 15-cm LD_2 target.

JLab Experimental Hall	**C**	A
Four-Momentum Transfer, Q^2 (GeV/c)^2	**4.3**	4.3
HMS (HRS) angular acceptance:		
$\Delta\theta_e$ (mrad)	**± 27.5**	± 28
$\Delta\phi_e$ (mrad)	**± 71.9**	± 60
HMS (HRS) efficiency, ϵ_e (%)	**92.0**	92.0
HMS (HRS) Momentum Bite, $\Delta p_e/p_e$ (%)	**-3.0/+10.0**	-3.0/+4.5
Neutron polarimeter angular acceptance:		
$\Delta\theta_n$ (mrad)	**± 71.4**	± 71.4
$\Delta\phi_n$ (mrad)	**± 85.5**	± 85.5
Neutron polarimeter efficiency, ϵ_n (%)	**0.91**	0.91
Beam Current, I_{beam} (μA)	**100**	100
MCEEP rate, $< R_{MCEEP} >$ (Hz)	**73.7**	47.1
Real-event rate, R_{real} (Hz)	**0.62**	0.39
Neutron polarimeter analyzing power, A_Y	**0.06**	0.06
Precession Angle, χ (deg)	**25**	25
Expected asymmetries:		
for -χ precession (%)	**-0.7**	-0.7
for +χ precession (%)	**1.6**	1.6

Table 2: The neutron polarimeter and HMS (HRS) acceptances, estimated neutron polarimeter parameters, and calculated real event rate at $Q^2 = 4.3$ (GeV/c)^2 for a beam current of 100 μA incident on a 15-cm LD_2 target in JLab Halls C and A. Also listed are the simulated NPOL efficiency and analyzing power (see Section 5 and Fig. 25 for details), and expected asymmetries for -χ and +χ precession of the neutron polarization vector.

in Hall C (A). [Note: We considered the HRS tune with the quads slid forward; this tune gives nearly twice the vertical acceptance and about one-third more horizontal acceptance. The momentum resolution decreases by an amount that is roughly proportional to the increase in vertical acceptance. We can not use this tune because the maximum momentum is restricted to $\sim$ 2.4 GeV/c.]

4.5 Projected Uncertainties

To estimate statistical uncertainties, we use the simple pairwise analysis here, but the actual analysis in the experiment will include acceptance averaging using methods similar to E93-038.

The up-down asymmetry, measured in JLab E93-038, is proportional to the projection of the neutron polarization vector on the axis that is perpendicular to the neutron momentum direction. Thus, the ratio of asymmetries for neutron spin precession through $\pm\chi$ degrees is given by:

$$\eta \equiv \frac{\xi_-}{\xi_+} = \frac{P^x_-}{P^x_+} = \frac{P_{S'}cos(-\chi) + P_{L'}sin(-\chi)}{P_{S'}\ cos(\chi) + P_{L'}\ sin(\chi)} = \frac{(P_{S'}/P_{L'})\ cos(\chi) - sin(\chi)}{(P_{S'}/P_{L'})\ cos(\chi) + sin(\chi)} \tag{10}$$

$$(P_{S'}/P_{L'}) = \frac{-sin(\chi)\ (\eta+1)}{cos(\chi)\ (\eta-1)} = -tan(\chi)\ \frac{(\eta+1)}{(\eta-1)} \tag{11}$$

where $P_{S'}$ and $P_{L'}$ are transverse and longitudinal projections of the neutron polarization vector:

$$P_{S'} \; = \; -h \; P_e \; \frac{K_S \; g}{K_0 \; (1 \; + \; g^2/K_0)} \tag{12}$$

$$P_{L'} \; = \; h \; P_e \; \frac{K_L}{K_0 \; (1 \; + \; g^2/K_0)} \tag{13}$$

Here h is the beam helicity, P_e is the beam polarization, and $g \equiv (G_E/G_M)$.

$$(P_{S'}/P_{L'}) \; = \; -g \; (K_S/K_L) \tag{14}$$

From (14) and (11) :

$$g \; = \; -\left(\frac{K_L}{K_S}\right) \left(\frac{P_{S'}}{P_{L'}}\right) \; = \; \left(\frac{K_L}{K_S}\right) \; tan(\chi) \; \frac{(\eta+1)}{(\eta-1)} \tag{15}$$

The statistical uncertainty in the g value is:

$$(\delta g)_{stat} \; = \; \left(\frac{K_L}{K_S}\right) \; tan(\chi) \; \frac{2}{(\eta-1)^2} \; \delta\eta \tag{16}$$

The relative statistical uncertainty $(\delta g/g)_{stat}$ is:

$$\left(\frac{\delta g}{g}\right)_{stat} \; = \; \frac{2}{(\eta+1)(\eta-1)} \; \delta\eta \tag{17}$$

Here $\delta\eta$ is the statistical error in the asymmetry ratio:

$$\left(\frac{\delta\eta}{\eta}\right)^2 \; = \; \left(\frac{\delta\xi_-}{\xi_-}\right)^2 \; + \; \left(\frac{\delta\xi_+}{\xi_+}\right)^2 \tag{18}$$

or

$$(\delta\eta)^2 \; = \; \left(\frac{\delta\xi_-}{\xi_+}\right)^2 \; + \; \xi_-^2 \left(\frac{\delta\xi_+}{\xi_+^2}\right)^2 \tag{19}$$

To project the statistical uncertainties, we used the statistical errors for asymmetries which come from Poisson statistics:

$$\left(\frac{\delta\xi_\pm}{\xi_\pm}\right)^2 \; = \; \frac{1}{\xi_\pm^2} \; \left(\frac{1+2/r}{N_\pm}\right) \; = \; \frac{1}{(A_Y P_\pm^x)^2} \; \left(\frac{1+2/r}{N_\pm}\right) \tag{20}$$

Here $N_\pm$ is the number of events taken during $\pm\chi$ precession angle runs, A_Y is the polarimeter analyzing power, and r is the ratio of real-to-accidental coincidences. For these projections, we used the value $r = 16.1$ from the simulation for a 100 μA beam at $Q^2 = 4.3$ (GeV/c)^2. To estimate accidental coincidence rates (~0.038 Hz), the electron single rate in the HMS (~0.80 kHz) was calculated with the MONQEE code (Dytman 1987), and the rate of coincidences in the front and the rear arrays of the polarimeter from inclusive neutrons (~24.0 kHz) was simulated with the program of P. Degtyarenko. This program, based on GEANT 3.21 (Brun 1993), uses the GCALOR (Zeitnitz 1994) program package in order to simulate hadronic interactions down to 1 MeV for nucleons and charged pions and into the thermal region for neutrons, and uses DINREG (Degtyarenko 1992, 2000) – Deep Inelastic Nuclear Reaction Exclusive Generator with a model for hadronic interactions of electrons and photons. Values of r achieved in E93-038 are compared

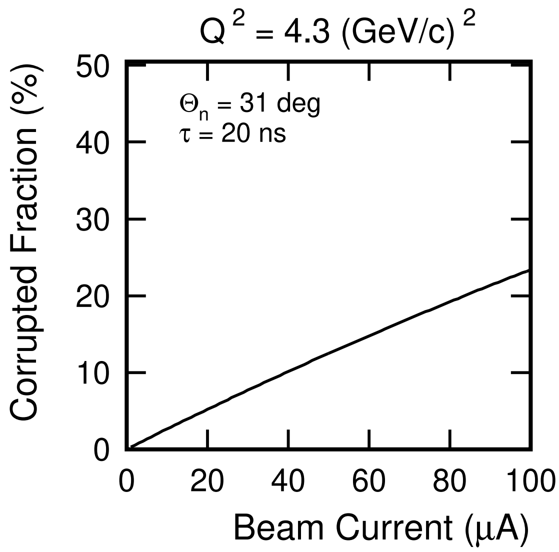

Figure 17: Calculated fraction of electron-neutron coincidence events corrupted from a background particle (charged or neutral) that appears during the coincidence time window of 20 ns as a function of the beam current.

with the results of simulation in Fig. 24. Using the single rates of neutral and charged particles in the front array of the polarimeter from the simulation with the program of P. Degtyarenko (see Fig. 16), we calculated a fraction of electron-neutron coincidence events corrupted from background particles. We consider a "good" neutron scattering event to be "corrupted" if the background particle (charged or neutral) appears near to the "good" neutron hit (ΔY = $\pm$25 cm) during a coincidence time window of 20 ns. For a 100 μA beam at $Q^2 = 4.3$ (GeV/c)^2, the corrupted fraction is calculated to be about 23% (see Fig. 17).

The projected uncertainties $\Delta g_n/g_n$ and ΔG_E^n are plotted in Fig. 18 as a function of the data acquisition time at $Q^2 = 4.3$ (GeV/c)^2 for a luminosity of 4.77×10^{38} cm^{-2}s^{-1}, which is achievable with a beam current of 100 μA on a 15-cm liquid deuterium target. The DAQ time that is designated by the dotted line in Fig. 18 was chosen to target an uncertainty ΔG_E^n in the vicinity of 0.0020.

Figure 19 shows the statistical uncertainty $\Delta g/g$, projected at $Q^2 = 4.3$ (GeV/c)^2 for the DAQ time of 528 hours as a function of precession angle χ.

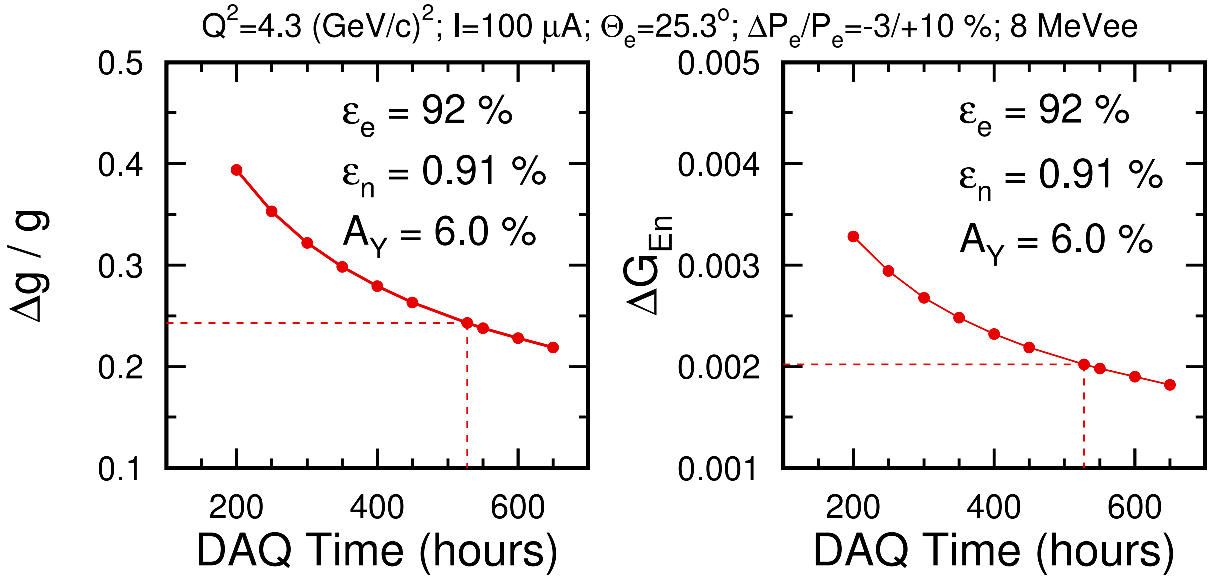

Figure 18: Projected uncertainties $\Delta g_n/g_n$ and ΔG_E^n at $Q^2 = 4.3$ (GeV/c)^2 for a beam current of 100 μA as a function of the DAQ time in Hall C.

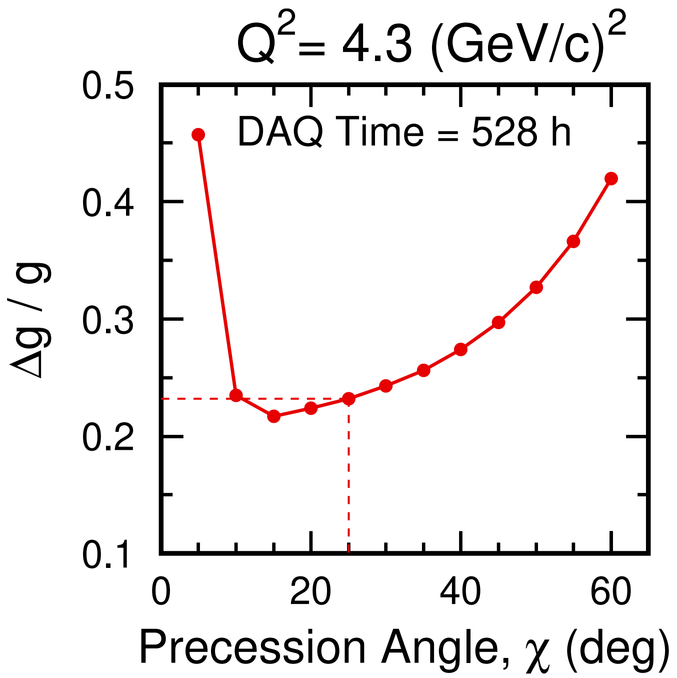

Figure 19: Statistical uncertainty $\Delta g/g$, projected at $Q^2 = 4.3$ (GeV/c)^2, as a function of precession angle χ.

5 Some Results from E93-038

The purpose of this section is to indicate the quality of the data obtained and the simulation made in E93-038. We selected real quasielastic ${}^2H(\vec{e}, e'n)$ events using a restricted HMS momentum bite, the cut on the missing momentum, and the cut on HMS-NPOL coincidence time (see Fig. 20). Typical time-of-flight spectra for the highest Q^2 [viz., $Q^2 = 1.45$ (GeV/c)^2] are shown

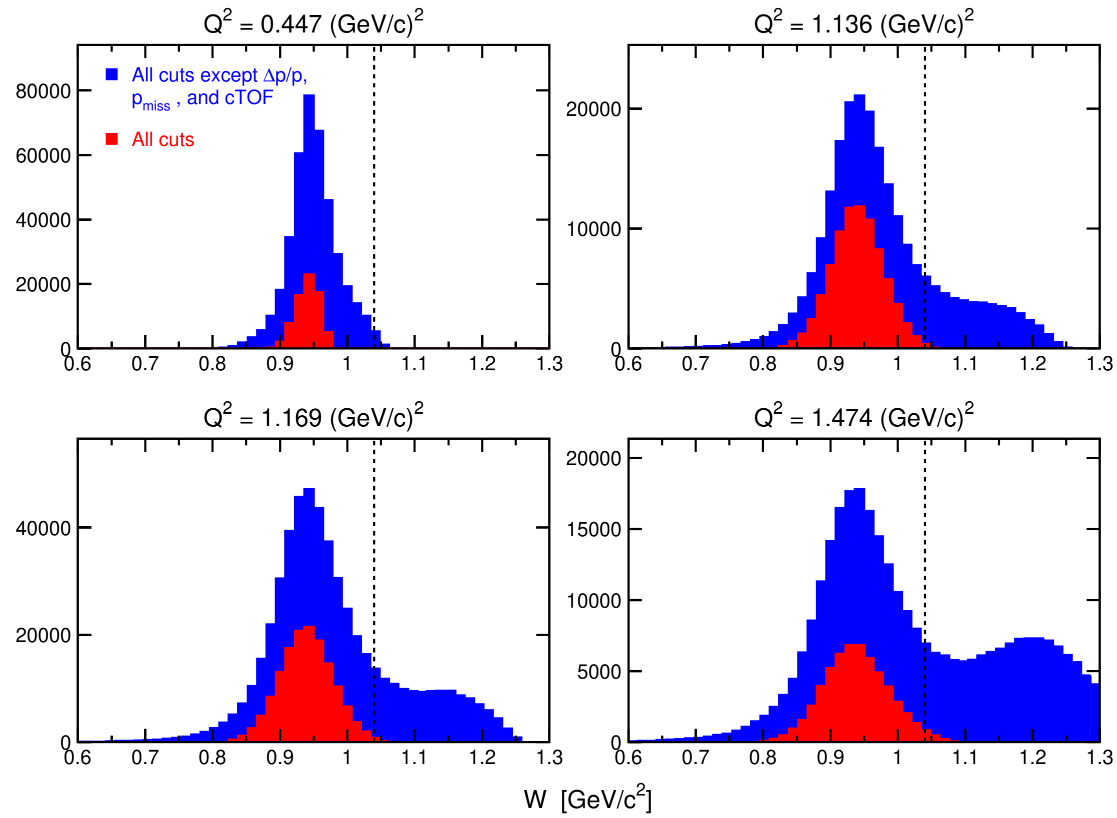

Figure 20: Invariant mass spectra before and after cuts on the scattered electron momentum, the missing momentum, and an HMS-NPOL coincidence time-of-flight.

in Fig. 21. The left panel is an HMS-NPOL coincidence time-of-flight spectrum. We compared the measured time-of-flight, cTOF, with the time-of-flight calculated from electron kinematics and offsets determined by a calibration procedure; the result is centered on zero with a FWHM of approximately 1.5 ns, and the reals-to-accidentals ratio is ≈ 12 at a beam current of ≈ 50 μA [see Fig. 24]. The right panel is the time-of-flight spectrum between a neutron event in the front array and an event in the top or bottom rear array. We compared this measured time-of-flight, ΔTOF, with the time-of-flight calculated for elastic np scattering. This result, normalized to the nominal 2.5 m flight path, has a peak at zero also. The tail on the slow side is due to scattering from carbon, and the secondary peak at ~ -2.5 ns is the result of π^0 production in the front array. To extract the physical scattering asymmetry, we calculated the cross ratio, r, which is defined to be the ratio of two geometric means, $(N_U^+ N_D^-)^{1/2}$ and $(N_U^- N_D^+)^{1/2}$, where $N_U^+(N_D^-)$ is the yield in the ΔTOF peak for neutrons scattered up(down) when the beam helicity was positive(negative); the yields, corrected for background, were obtained by peak fitting. The physical scattering asymmetry is then given by $(r-1)/(r+1)$. The merit of the cross ratio technique [Ohlsen (1973)] is that the neutron polarimeter results are independent of the luminosities for positive and negative helicities, and the efficiencies and acceptances of the top and bottom halves of the polarimeter. Beam charge asymmetries (of typically 0.1%) and detector threshold differences cancel in the cross ratio. The result of an analysis of the asymmetries for each run

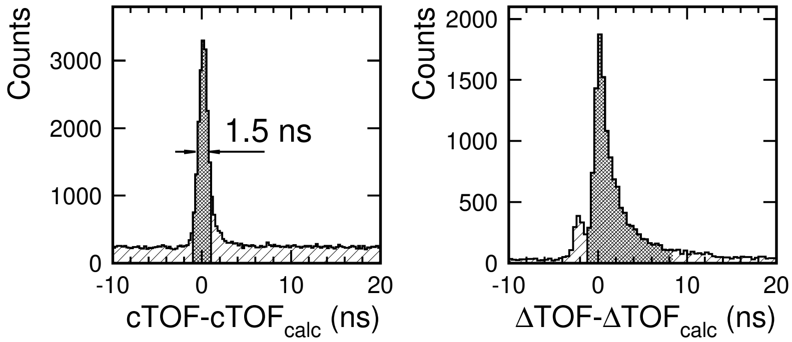

Figure 21: Typical time-of-flight spectra for $Q^2 = 1.45$ (GeV/c)^2. Selected portions are shaded.

at $Q^2 = 1.13$ (GeV/c)^2 and the error-bar weighted average for these data appear in Fig. 22; the sign of the asymmetries from runs with the $\lambda/2$-plate IN have been reversed. A histogram of the asymmetries (see Fig. 23) clearly demonstrates that the distribution of the asymmetries is of an appropriate Gaussian shape.

To estimate reals-to-accidentals ratio r, we simulated the rate of inclusive electrons in HMS with MONQUEE code [Dytman (1987)], and we used single rates in NPOL simulated with the GEANT-based program of P. Degtyarenko (for details, see Section 4.5). Simulated accidental coincidence rates and r-values are shown in Fig. 24 together with ones measured in E93-038. The large difference between the measured and calculated accidentals and the ratios of real-to-accidental coincidences at $Q^2 = 0.45$ (GeV/c)^2 is because the calculation doesn't take into account the larger radiation background in Hall C caused by multiple scattering of electrons at this lowest beam energy of 884 MeV.

We simulated the E93-038 neutron polarimeter efficiency, ϵ_n, (including a neutron transmission through 10-cm lead curtain) using the FLUKA-2002 program, version 2.0 [Fasso et al. (2001)]. The "stand-alone" (not GEANT-based) FLUKA-2002 code is a general purpose Monte Carlo code for studying transport and interactions of particles in a material over a wide energy range. The program is best known for its hadron event generators; the used version of the code can also handle (with similar or better accuracy) muons, low-energy neutrons, and electromagnetic effects. Figure 25 (left panel) indicates good agreement of the results of the simulation with NPOL efficiencies extracted from E93-038 data [Semenova et al. (2003)]. Both simulation and data analysis were made for the front (rear) array threshold of 8 (20) MeVee. Simulating the analyzing power (A_Y) for E93-038 polarimeter, for elastic *n-p* and quasielastic scattering events in the front array, we determined (*in the rest frame of the target nucleon*) A_Y values from the partial-wave analysis embodied in the Scattering Analysis Interactive Dial-In (SAID) code [Arndt (1977, 2000)]. In our simplified approach, we supposed that $A_Y = 0$ for both inelastic reactions and multiple scattering events. Probably, this assumption leads to the disagreement between the simulated (and averaged over the NPOL acceptance) and the measured analyzing power at the low neutron energy of 239 MeV. Nevertheless, at higher neutron energies ($T_n = 608$ and 786 MeV), *the simulated and measured in E93-038* A_Y *values are in very good agreement* (see right panel in Fig. 25).

The beam polarization measured in March 2001 is plotted in Fig. 26. The mean polarization during this two-weeks period was 82.2±0.1 (-81.0±0.2)% with the $\lambda/2$ wave plate "OUT" ("IN").

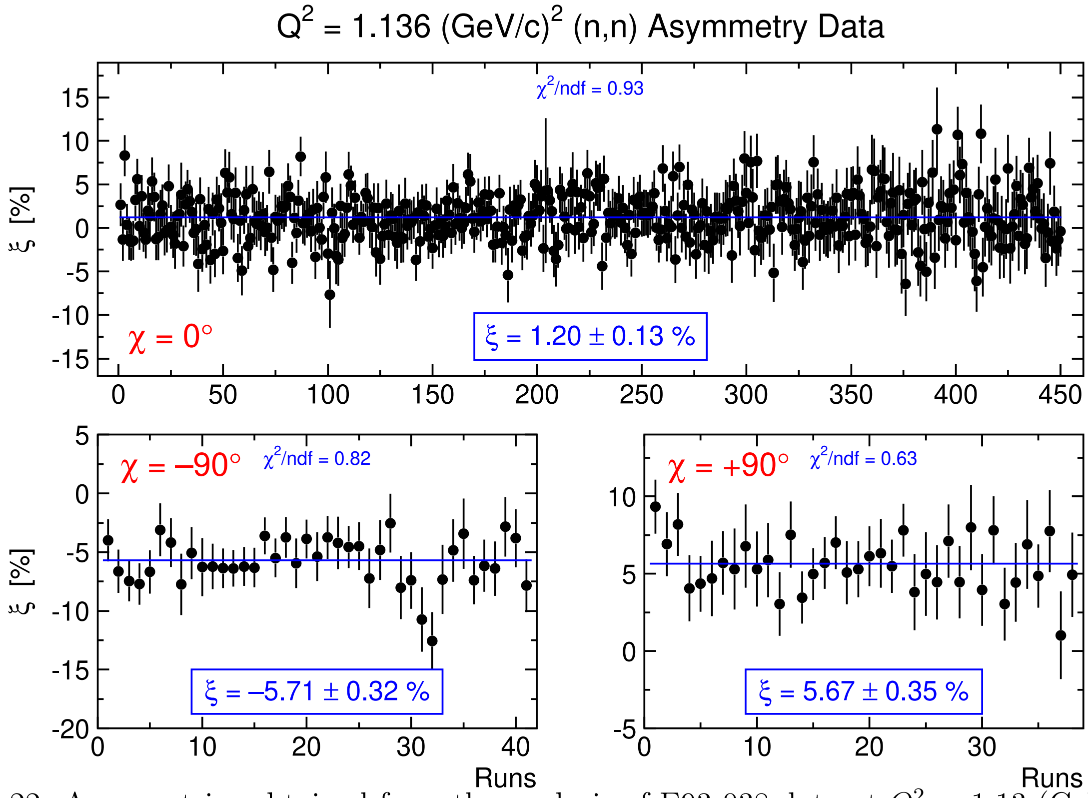

Figure 22: Asymmetries obtained from the analysis of E93-038 data at $Q^2 = 1.13$ (GeV/c)^2.

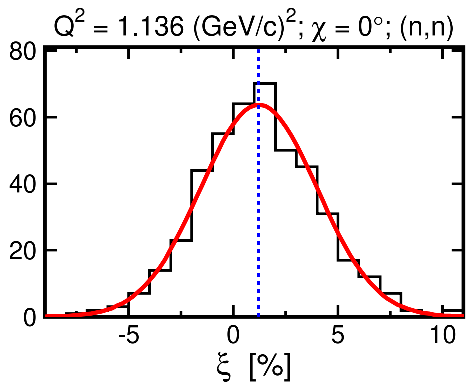

Figure 23: Histogram of E93-038 asymmetries at $Q^2 = 1.13$ (GeV/c)^2 ($\chi = 0^o$). The red solid curve is a Gaussian fit, and the blue dashed line is the mean value of the asymmetry from the Fig. 22.

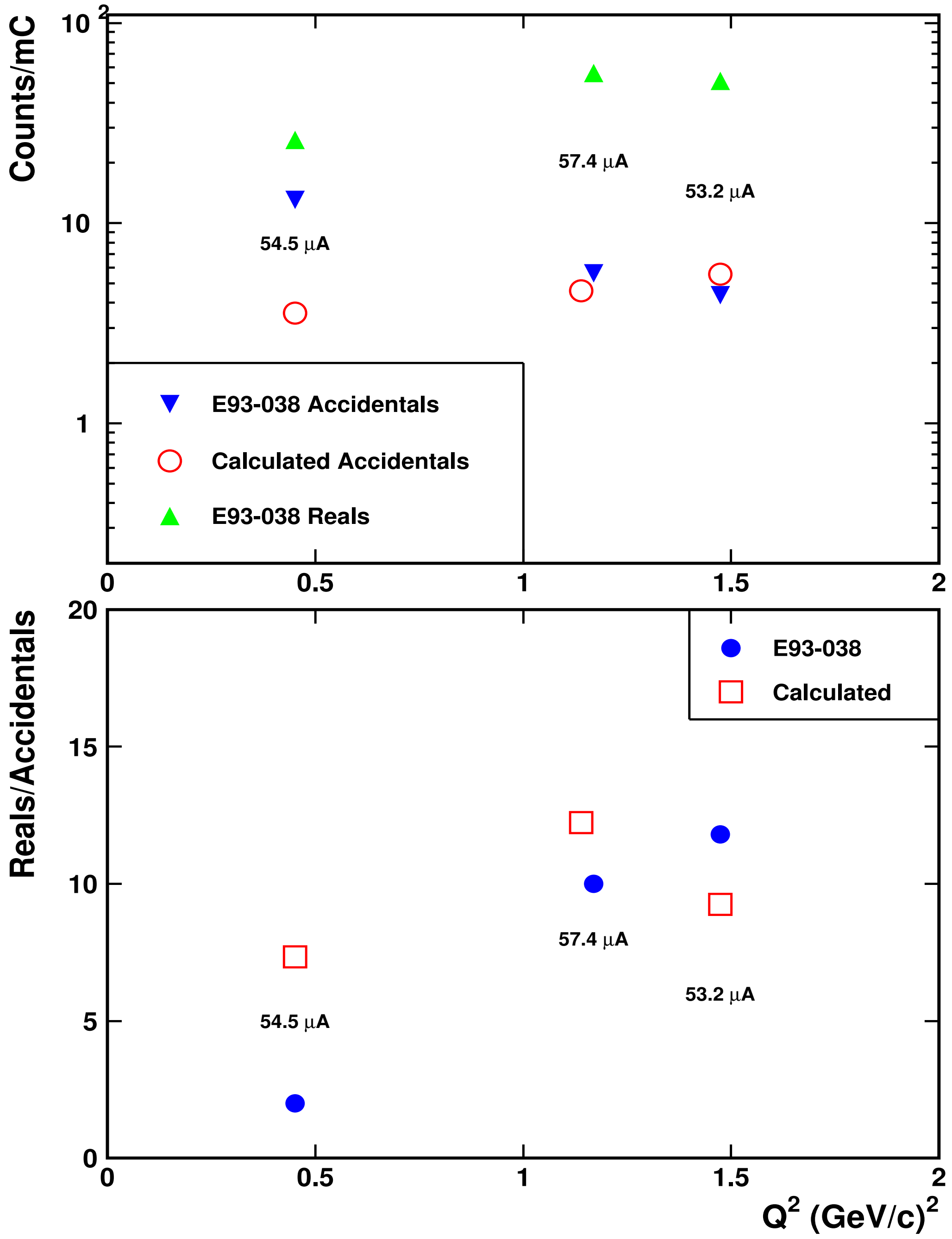

Figure 24: Real event rate, accidental coincidence rate, and the reals-to-accidentals ratio obtained from E93-038. The target-front array flight path was 7 m for NPOL at 46 degrees.

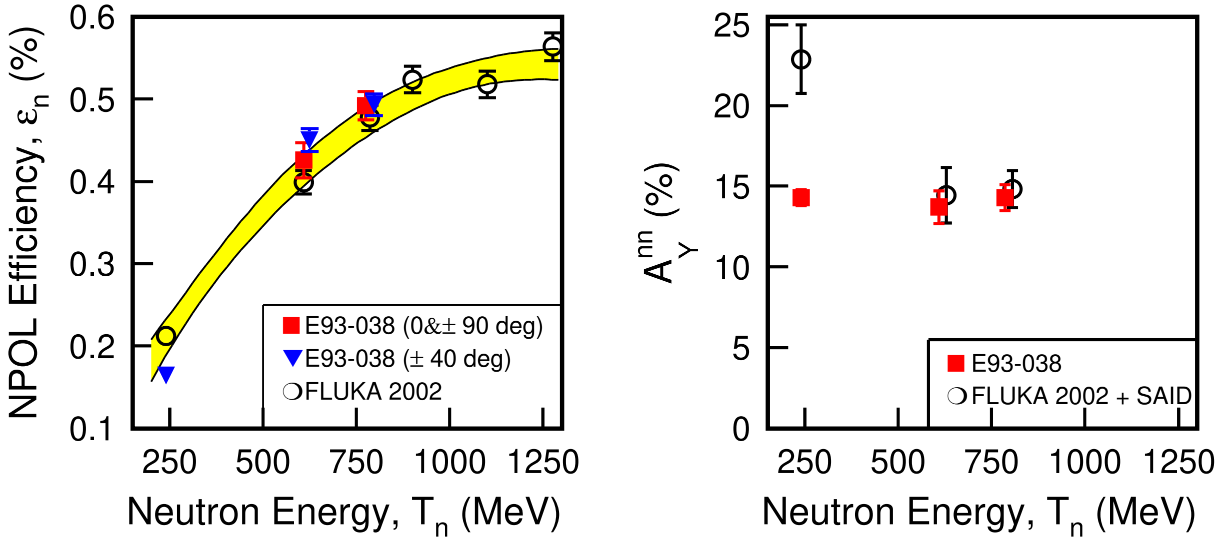

Figure 25: Comparison of the simulated neutron polarimeter parameters (viz., analyzing power, A_Y, and the neutron polarimeter efficiency, ϵ_n) with the results from E93-038. Yellow band in the left panel shows an uncertainty on the fit of the simulated efficiencies with a polynomial function.

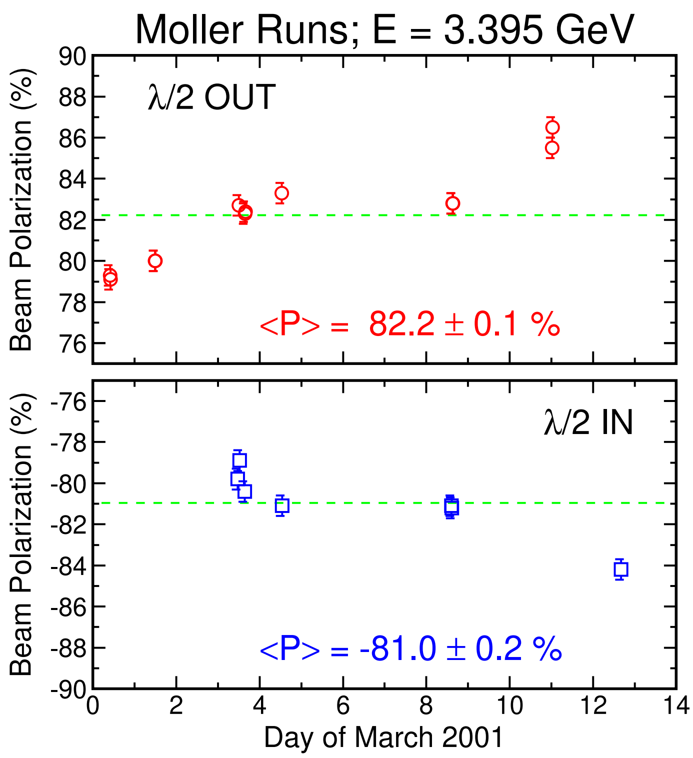

Figure 26: Electron beam polarization in March 2001.

6 Beam Time

Our beam-time request for measuring G_E^n at $Q^2 = 4.3$ (GeV/c)^2 is shown in Table 3. We estimate that a total data acquisition time of 25 days *in Hall C* will be needed to produce a statistical uncertainty ΔG_E^n in the vicinity of 0.0020 at $Q^2 = 4.3$ (GeV/c)^2. The projection was based on a calculation of a fraction of electron-neutron coincidence events corrupted from a background particle (charged or neutral) that appears during a coincidence time window of 20 ns. For a 100 μA beam at $Q^2 = 4.3$ (GeV/c)^2, the corrupted fraction is calculated to be about 23% (see Fig. 17). The estimated acquisition times for runs on a 15-cm LH_2 target will be needed to assess the false asymmetry or dilution from the two-step process d($\vec{e}$,e'$\vec{p}$)n + Pb($\vec{p}$,$\vec{n}$).

G_E^n physics measurements Q^2 [(GeV/c)^2]	4.3
LD_2 target	22
LH_2 target	0.7
Dummy target	0.3
Beam polarization	1
Time calibrations [LD_2 target]	0.5
Overhead [(a)]	0.5
Total physics measurements	25

Table 3: Beam-time [days] for measuring at $Q^2 = 4.3$ (GeV/c)^2 for a 100 μA, 80% polarized beam on a 15-cm LD_2 target.

(a) 40 changes in Charybdis dipole current, 9 target changes, starting and stopping the DAQ system at least 105 times for runs that are typically 5 hours long.

Also needed will be seven days of commissioning time with beam to check out the spectrometer, the Moeller polarimeter, and the neutron polarimeter [NPOL] and electronics. NPOL checkout includes checking all detectors and detector thresholds, adjusting timing, adjusting the thickness of the Pb curtain and determining the optimal beam current, and checking room background with a shadow shield. Seven days will be required without beam for pulse-height calibrations and cosmic ray tests of the polarimeter detectors.

The proposed measurements can be done also *in Hall A*. The limited momentum bite and slightly smaller angular acceptance of HRS leads to about 64% (see Table 2) of the count rate in the Hall C. We estimate that we will produce a statistical uncertainty ΔG_E^n in the vicinity of 0.0025 with 25 days total DAQ time in Hall A. If this uncertainty is acceptable to the PAC, this collaboration is willing to run in Hall A if the scheduling constraints are less stringent there.

7 Prospects for Measurements with Upgraded CEBAF

The energy upgrade of the accelerator offers an oportunity to reach higher values of Q^2; for example, a Q^2 of 6 (GeV/c)^2 can be reached with a 10-GeV incident beam. The kinematics for this case put the neutron polarimeter at 29.7 deg and the HMS at 17.08 deg; the central electron momentum of 6.8 GeV/c is below the maximum central momentum in HMS of 7.5 GeV/c. The statistical uncertainty that might be achieved will depend on the value of the analyzing power A_Y and the polarimeter efficiency ϵ for neutrons of 3.2 GeV. Our extraction of A_Y and ϵ from the proposed measurement at $Q^2 = 4.3$ (GeV/c)^2 will enable us to make a more reliable extrapolation of A_Y and ϵ to $Q^2 = 6.0$ (GeV/c)^2. Assuming A_Y and ϵ do not decrease, we project a real event rate of ~0.45 Hz and a statistical uncertainty $\Delta G_E^n \approx 0.0019$ in 30 days in Hall C.

With a 10.9-GeV incident beam, it is possible to reach a $\mathbf{Q^2} = \mathbf{6.5}$ (GeV/c)^2 with neutron polarimeter at 29.0 deg and the HMS at 16.3 deg; the central electron momentum is 7.44 GeV/c.

8 Collaboration

Each of the participants listed earlier contributed to the success of E93-038. The collaboration is a strong, experienced, and large team (currently about 70 scientists from 26 institutions). Graduate students and postdocs will be added after the proposed experiment is approved and scheduled. As in E93-038, Kent State University (KSU) will be responsible for the neutron polarimeter; MIT, for the neutron spin-precession dipole magnet [CHARYBDIS]; and JLab for the magnetic spectrometer [HMS]. KSU provided the neutron detectors in the rear array and the polarimeter electronics; Hampton University provided ten of the neutron detectors in the front array, while JLab provided another ten. We need another 55 of these 10-cm×10-cm×100-cm detectors. The University of Virginia provided the tagger detectors used in E93-038. Duke University took responsibility for the Analysis Engine and also for setting up the electronics and timing. Professor James J. Kelly at the University of Maryland spearheaded the development of the analysis programs used in E93-038, and Dr. A.Yu. Semenov functioned as the coordinator of the E93-038 analysis effort. T. Reichelt (Bonn), H. Fenker (JLab), and S. Danagoulian (NCAT) were the lead scientists in establishing the operating conditions for running the Moeller polarimeter at a beam energy below one GeV, and in setting up and running the Moeller polarimeter at the two higher energies. A. Ahmidouch (NCAT) and S. Taylor (MIT) were the lead scientists in mapping the CHARYBDIS dipole magnet. For this proposal, the personnel at the same institutions will provide their expertise. With respect to the rear array, we are planning to replace the 12 [20-in×40-in×4-in] detectors in the rear array with 24 [10-in×40-in×4-in] detectors; to do so, Kent State University will make two nominally 10-in wide detectors from each 20-in wide detector. A recent price quote from Saint-Gobain [Bicron] for scintillators (with machined and polished light pipes on each end) is $1400 for each [10-cm×10-cm×100-cm] bar; the total cost for 43 such detectors would be $60,200. KSU will assemble and test the detectors. We will need several photomultiplier tubes (PMT's): For the 60 detectors in the front array, we need 128 [including 8 spares of Hamamatsu R1828-01, 2-in diam] PMT's at a cost of $107,500; and for the 24 [10-in×40-in×4-in] detectors in the rear array, we need 50 [including 2 spares of Hamamatsu R1250, 5-in diam] PMT's at a cost of $108,000. For the two layers of veto detectors ahead of the front array, we need a total of 26 (including 2 spares) [106 cm long×10 cm high×1 cm] thick scintillators with a light pipe and a PMT (with a magnetic shield) on each end. The cost for the front veto detectors is $23,100. For the rear vetos, we need a total of 10 (including 2 spares) 160 cm long×50 cm wide×1 cm thick scintillators with an adiabatic light pipe and a PMT (with a magnetic shield) on each end. The cost of the rear veto detectors is $29,000. KSU will assemble and test these new veto detectors. The cost of 138 additional magnetic shields [Hamamatsu E989-41 for the R1828-01 2-in diam PMT] for the front array is $18,600; the cost of 68 additional magnetic shields [Hamamatsu E989-32 for the R1250 5-in PMT] for the rear array is $17,000. New electronics needs for the enhanced polarimeter include 10 quad constant fraction discriminators at a cost of $28,000, 36 (400 ns) delay lines, an additional control box, and 125 (including 5 spares) PMT bases and preamps for the front array and additional PMT bases for other detectors. We are requesting JLab to provide the quad constant-fraction discriminators, and the delay lines; KSU would provide the preamps, the control box, and the PMT bases. In the enhanced polarimeter, we plan to use multi-hit TDC's, which we understand are available now at JLab.

Equipment items that need to be purchased are summarized in Table 4. Funds will be sought from DOE and NSF by the participating institutions.

	Cost
1. **Front Array**	
1.1 43 [10 cm × 10 cm × 100 cm] Scintillators & Light Pipes	\$60,200
1.2 26 [1 cm × 10 cm × 106 cm] Veto Scintillators & Light Pipes	\$23,100
1.3 178 Photomultiplies Tubes (2-in diam)	\$149,500
1.4 138 Magnetic Shields (for 2-in diam PMT)	\$18,600
Subtotal Front Array	**\$251,400**
2. **Rear Array**	
2.1 10 [1 cm × 50 cm × 106 cm] Veto Scintillators & Light Pipes	\$29,000
2.2 70 Photomultiplies Tubes (5-in diam)	\$150,000
2.3 68 Magnetic Shields (for 5-in diam PMT)	\$17,000
Subtotal Rear Array	**\$196,000**
3. **Electronics**	
3.1 10 Quad Discriminators	\$28,000
Subtotal Electronics	**\$28,000**
Total	**\$475,400**

Table 4: NPOL equipment items to be purchased.

References

[Arenhoevel 1987] H. Arenhoevel, Phys. Lett. **B199**, 13 (1987).

[Arenhoevel 1988] H. Arenhoevel *et al.*, Z. Phys. **A331**, 123 (1988).

[Arenhoevel 2002] H. Arenhoevel, private communication (2002).

[Arndt 1977] R.A. Arndt, R.H. Hackman, and L.D. Roper, Phys. Rev. **C15** 1002 (1977).

[Arndt 2000] R. A. Arndt, L. D. Roper *et al.*, Scattering Analysis Interactive Dial-In (SAID) Program. Virginia Polytechnic Institute and State University, Unpublished. The Virginia Tech Partial-Wave Analysis Facility is still available from the original web site *http://said.phys.vt.edu/*. This facility is available on-line at *http://www.gwdac.phys.gwu.edu/* from the CNS Data Analysis Center at The George Washington University.

[Ashley 2004] J.D. Ashley *et al.*, hep-lat/0308024; submitted to EPJ.

[Aznaurian 1993] I.G. Aznaurian, Phys. Lett. **B316**, 391 (1993).

[Beck 1992] G. Beck and H. Arenhoevel, Few Body Systems **13**, 165 (1992).

[Bermuth 2003] J. Bermuth et al., Phys. Lett. **B564**, 199 (2003) updates D. Rohe *et al.*, Phys. Rev. Lett. **83**, 4257 (1999).

[Bijker 2004] R. Bijker and F. Iachello, nucl-th/0405026, accepted for publication in Phys. Rev. C (2004).

[Boffi 2002] S. Boffi, L. Ya. Glozman, W. Klink, W. Plessas, M. Radici, and R. F. Wagenbrunn, Eur. Phys. J. A **14**, 17 (2002); W. Plessas, S. Boffi, L. Ya. Glozman, W. Klink, M. Radici, and R. F. Wagenbrunn, Nucl. Phys. A **699**, 312c (2002); R. F. Wagenbrunn, S. Boffi, W. Klink, W. Plessas, and M. Radici, Phys. Lett. B **511**, 33 (2001).

[Brun 1993] R. Brun et al. *GEANT Detector Description and Simulation Tool*. CERN Program Library Long Writeup W5013, September, 1993.

[Cardarelli 2000] F. Cardarelli, S. Simula, Phys. Rev. **C62**, 065201 (2000); S. Simula (private communication).

[Cecil 1979] R. Cecil, B.D. Anderson, R. Madey. Nucl. Instrum. Meth. **161**, 439 (1979).

[Chung 1991] P.L. Chung and F. Coester, Phys. Rev. **D44**, 229 (1991).

[Degtyarenko 1992] P.V. Degtyarenko, M.V. Kossov. *Monte Carlo Program for Nuclear Fragmentation*. Preprint ITEF 11-92, Moskow (1992).

[Degtyarenko 2000] P.V. Degtyarenko, M.V. Kossov, and H.-P. Wellisch. *Chiral invariant phase space event generator*. Eur. Phys. J. A **8**, 217-222 (2000); A **9**, 411-420 (2000); A **9**, 421-424 (2000).

[Dong 1998] S.J. Dong, K.F. Liu, and A.G. Williams, Phys. Rev. **D58**, 074504 (1998).

[Drechsel 1989] D. Drechsel and M.M. Giannini, Rep. Prog. Phys. **52**, 1083 (1989).

[Dytman 1987] S. Dytman, private communication (1987).

[Eden 1994] T. Eden *et al.*, Phys. Rev. **C50**, R1749 (1994).

[Fasso 2001] A. Fasso, A. Ferrari, P.R. Sala, Electron-Photon Transport in FLUKA: Status, Proceedings of the Monte Carlo 2000 Conference, Lisbon, October 23-26, 2000, A. Kling, F. Barao, M. Nakagawa, L. Tavora, P. Vaz eds., Springer-Verlag Berlin, pp. 159-164 (2001).

[Fasso 2001a] A. Fasso, A. Ferrari, J. Ranft, P.R. Sala, FLUKA: Status and Perspective for Hadronic Applications, Proceedings of the Monte Carlo 2000 Conference, Lisbon, October 23-26, 2000, A. Kling, F. Barao, M. Nakagawa, L. Tavora, P. Vaz eds., Springer-Verlag Berlin, pp. 955-960 (2001).

[Feshbach 1967] H. Feshbach and E. Lomon, Rev. Mod. Phys. **39**, 611 (1967).

[Frank 1996] M.R. Frank, B.K. Jennings, and G.A. Miller, Phys. Rev. **C54**, 920 (1996).

[Friar 1990] J.L. Friar, Phys. Rev. **C42**, 2310 (1990).

[Gari 1985] M.F. Gari and W. Krumpelmann, Z. Phys. **A322**, 689 (1985).

[Gari 1992] M.F. Gari and W. Krumpelmann, Phys. Lett. **B274**, 159 (1992).

[Galster 1971] S. Galster, H. Klein, J. Moritz, K.H. Schmidt, D. Wegener, and J. Bleckwenn, Nucl. Phys. **B32**, 221 (1971).

[Gayou 2002] O. Gayou *et al.*, Phys. Rev. Lett. **88**, 092301 (2002).

[Golack 2001] J. Golak, G. Ziemer, H. Kamada, H. Witala, and W. Glöckle, Phys. Rev. C **63**, 034006 (2001) applies FSI corrections to J. Becker *et al.*, Eur. Phys. J. A **6**, 329 (1999).

[Herberg 1999] C. Herberg *et al.*, Eur. Phys. J. **A5**, 131 (1999) applies FSI corrections to M. Ostrick *et al.*, Phys. Rev. Lett. **83**, 276 (1999).

[Holzwarth 2002] G. Holzwarth, hep-ph/020138; Z. Phys. **A356**, 339 (1996).

[Iachello 1973] F. Iachello, A.D. Jackson, and A. Lande, Phys. Lett. **43B**, 191 (1973).

[Iachello 2003] F. Iachello, Proceedings of 4th Int. Conference on Perspectives in Hadronic Physics, Trieste, Italy (2003). To be published in Eur. Phys. J.

[Isgur 1998] N. Isgur, Phys. Rev. Lett. **83**, 272 (1999).

[Isgur 2000] N. Isgur and J.W. Negele, Nuclear Theory with Lattice QCD, a proposal to DOE, PI's (2000).

[Ji 1991] X. Ji, Phys. Lett. **B254**, 456 (1991).

[Jones 2000] M. Jones *et al.*, Phys. Rev. Lett. **84**, 1398 (2000).

[Kaskulov (2003)] M.M. Kaskulov and P. Grabmayr, Phys. Rev. C **67**, 042201(R) (2003); nucl-th/0308105; M.M. Kaskulov (private communication).

[Kelly 2000] J.J. Kelly, GENGEN: Event Generator for Gen Using the d(e,e'n)p Reaction, JLab E93-038 internal report (2000), URL: *http://www.jlab.org/ semenov/reports/gengen2.5.ps*

[Kelly 2001a] J.J. Kelly, Time Calibration Procedures for E93-038 Polarimeter: Version 2.2, JLab E93-038 internal report (2001), URL: *http://www.physics.umd.edu/enp/e93038/time_calibration.ps*

[Kelly 2003] J.J. Kelly, private communication (2003).

[Klein 1997a] F. Klein and H. Schmieden, Nucl. Phys. **A623**, 323c (1997).

[Klein 1997b] F. Klein, Proc. of the 14th Int. Conf. on Particles and Nuclei, ed. by C.E. Carlson and J.J. Domingo, World Scientific 1997, p.121.

[Kopecky 1997] S. Kopecky *et al.*, Phys. Rev. C **56**, 2229 (1997); Phys. Rev. Lett. **74**, 2427 (1995).

[Kroll 1992] P. Kroll, M. Schurmann, and W. Schweiger, Z. Phys. **A342**, 429 (1992).

[Laget 1990] J.M. Laget, Phys. Lett. **B273**, 367 (1990).

[Liu 2001] K.F. Liu, Private Communication (2001).

[Lomon 2002] E. L. Lomon, Phys. Rev. C **66**, 045501 (2002); Phys. Rev. C **64**, 035204 (2001).

[Lu 1998] D.H. Lu, A.W. Thomas, and A.G. Williams, Phys. Rev. **C57**, 2628 (1998).

[Lung 1993] A. Lung *et al.*, Phys. Rev. Lett. **70**, 718 (1993).

[Ma 2002] B.-Q. Ma, D. Qing, and I. Schmidt, Phys. Rev. C **65**, 035205 (2002).

[Madey 1995] R. Madey, A. Lai, and T. Eden, Polarization Phenomena in Nuclear Physics, edited by E.J. Stephenson S.E. Vigelor, AIP Proceedings No. 339, 47-54 (1995).

[Madey 2003] R. Madey *et al.*, Phys. Rev. Lett. **91**, 122002 (2003).

[Mergell 1996] P. Mergell, U.G. Meissner, D. Drechsel , Nucl. Phys. **A596**, 367 (1996).

[Meyerhoff 1994] M. Meyerhoff *et al.*, Phys. Lett. **B327**, 201 (1994).

[Milbrath 1998] B. D. Milbrath *et al.*, Phys. Rev. Lett. **80**, 452 (1998); Phys. Rev. Lett. **82**, 2221(E) (1999).

[Miller 2002] G. A. Miller, Phys. Rev. C **66**, 032201(R) (2002); nucl-th/0206027; G. A. Miller and M. R. Frank, Phys. Rev. C **65**, 065205 (2002); M. R. Frank, B. K. Jennings, and G. A. Miller, Phys. Rev. C **54**, 920 (1996); G. A. Miller, private communication (2003).

[Mosconi 1991] B. Mosconi, J. Pauchenwein, and P. Ricci, Proceedings of the XIII European Conference on Few-Body Problems in Physics, Marciana Marina (Elba), Italy (September 1991).

[Ohlsen 1973] G.G. Ohlsen and P.W. Keaton, Jr., Nucl. Instr. Meth. **109**, 41 (1973).

[Pace 2000] E. Pace, G. Salme, F. Cardarelli, and S. Simula, Nucl. Phys. **A666**, 33 (2000).

[Passchier 1999] I. Passchier *et al.*, Phys. Rev. Lett. **82**, 4988 (1999).

[Platchkov 1990] S. Platchkov *et al.*, Nucl. Phys. **A508**, 343c (1990).

[Pospischil 2001] Th. Pospischil *et al.*, Eur. Phys. J. A **12**, 125 (2001).

[Radyushkin 1984] A.V. Radyushkin, Acta Phys. Polon. **B15**, 403 (1984).

[Rekalo 1989] M.P. Rekalo, G.I. Gakh, and A.P. Rekalo, J. Phys. **G15**, 1223 (1989).

[De Sanctis 2000] M. De Sanctis, M.M. Giannini, L. Repetto, and E. Santopinto, Phys. Rev. **C62**, 025208 (2000).

[Schiavilla 2001] R. Schiavilla and I. Sick, Phys. Rev. **C64**, 041002 (2001).

[Schmieden 1996] H. Schmieden, Proc. of the 12th Int. Symposium on High-Energy Spin Physics, Amsterdam (1996), ed. by C.W. de Jager et al., World Scientific 1997, p.538.

[Semenova 2002] I.A. Semenova, R. Madey, and A.Yu. Semenov, Gain in Figure-of-Merit of the E93-038 Neutron Polarimeter with Passive Converters, JLab E93-038 internal report (2002),
URL: *http://www.jlab.org/∼semenov/reports/irina-effConv.ps*

[Semenova 2003] I.A. Semenova, A.Yu. Semenov, and R. Madey, Simulation of the Efficiency of the E93-038 Neutron Polarimeter with the FLUKA code, JLab E93-038 internal report (2003).

[Thomas 2003] A.W. Thomas *et al.*, Nucl. Phys. **A721**, 915 (2003).

[Ulmer 1991] P.E. Ulmer, MCEEP – Monte Carlo for Electro-Nuclear Coincidence Experiments, CEBAF–TN–91–101 (1991).

[Zeitnitz 1994] C. Zeitnitz and T.A. Gabriel, Nucl. Instrum. Meth. **A349**, 106 (1994).

[Zhu 2001] H. Zhu *et al.*, Phys. Rev. Lett. **87**, 081801 (2001).

Appendix A

VOLUME 91, NUMBER 12 PHYSICAL REVIEW LETTERS week ending 19 SEPTEMBER 2003

Measurements of G_E^n/G_M^n from the $^2\mathrm{H}(\vec{e}, e'\vec{n})^1\mathrm{H}$ Reaction to $Q^2 = 1.45\ (\mathrm{GeV}/c)^2$

R. Madey,[1,2] A. Yu. Semenov,[1] S. Taylor,[3] B. Plaster,[3] A. Aghalaryan,[4] E. Crouse,[5] G. MacLachlan,[6] S. Tajima,[7] W. Tireman,[1] Chenyu Yan,[1] A. Ahmidouch,[8] B. D. Anderson,[1] H. Arenhövel,[9] R. Asaturyan,[4] O. K. Baker,[10] A. R. Baldwin,[1] D. Barkhuff,[3,*] H. Breuer,[11] R. Carlini,[2] E. Christy,[10] S. Churchwell,[7,†] L. Cole,[10] S. Danagoulian,[2,8] D. Day,[12] T. Eden,[1,10,‡] M. Elaasar,[13] R. Ent,[2] M. Farkhondeh,[3] H. Fenker,[2] J. M. Finn,[5] L. Gan,[10] K. Garrow,[2] A. Gasparian,[8,10] P. Gueye,[10] C. R. Howell,[7] B. Hu,[10] M. K. Jones,[2] J. J. Kelly,[11] C. Keppel,[10] M. Khandaker,[14] W.-Y. Kim,[15] S. Kowalski,[3] A. Lai,[1] A. Lung,[2] D. Mack,[2] D. M. Manley,[1] P. Markowitz,[16] J. Mitchell,[2] H. Mkrtchyan,[4] A. K. Opper,[6] C. Perdrisat,[5] V. Punjabi,[14] B. Raue,[16] T. Reichelt,[17] J. Reinhold,[16] J. Roche,[5] Y. Sato,[10] N. Savvinov,[11] I. A. Semenova,[1] W. Seo,[15] N. Simicevic,[18] G. Smith,[2] S. Stepanyan,[4,15] V. Tadevosyan,[4] L. Tang,[10] P. E. Ulmer,[19] W. Vulcan,[2] J. W. Watson,[1] S. Wells,[18] F. Wesselmann,[12] S. Wood,[2] Chen Yan,[2] S. Yang,[15] L. Yuan,[10] W.-M. Zhang,[1] H. Zhu,[12] and X. Zhu[10]

(The Jefferson Laboratory E93-038 Collaboration)

[1]*Kent State University, Kent, Ohio 44242, USA*
[2]*Thomas Jefferson National Accelerator Facility, Newport News, Virginia 23606, USA*
[3]*Massachusetts Institute of Technology, Cambridge, Massachusetts 02139, USA*
[4]*Yerevan Physics Institute, Yerevan 375036, Armenia*
[5]*The College of William and Mary, Williamsburg, Virginia 23187, USA*
[6]*Ohio University, Athens, Ohio 45701, USA*
[7]*Duke University and TUNL, Durham, North Carolina 27708, USA*
[8]*North Carolina A&T State University, Greensboro, North Carolina 27411, USA*
[9]*Johannes Gutenberg-Universität, D-55099 Mainz, Germany*
[10]*Hampton University, Hampton, Virginia 23668, USA*
[11]*University of Maryland, College Park, Maryland 20742, USA*
[12]*University of Virginia, Charlottesville, Virginia 22904, USA*
[13]*Southern University at New Orleans, New Orleans, Louisiana 70126, USA*
[14]*Norfolk State University, Norfolk, Virginia 23504, USA*
[15]*Kyungpook National University, Taegu 702-701, Korea*
[16]*Florida International University, Miami, Florida 33199, USA*
[17]*Rheinische Friedrich-Wilhelms-Universität, D-53115 Bonn, Germany*
[18]*Louisiana Tech University, Ruston, Louisiana 71272, USA*
[19]*Old Dominion University, Norfolk, Virginia 23529, USA*
(Received 27 June 2003; published 19 September 2003)

We report new measurements of the ratio of the electric form factor to the magnetic form factor of the neutron, G_E^n/G_M^n, obtained via recoil polarimetry from the quasielastic $^2\mathrm{H}(\vec{e}, e'\vec{n})^1\mathrm{H}$ reaction at Q^2 values of 0.45, 1.13, and 1.45 $(\mathrm{GeV}/c)^2$ with relative statistical uncertainties of 7.6% and 8.4% at the two higher Q^2 points, which points have never been achieved in polarization measurements.

DOI: 10.1103/PhysRevLett.91.122002 PACS numbers: 14.20.Dh, 13.40.Gp, 24.70.+s, 25.30.Bf

The nucleon elastic electromagnetic form factors are fundamental quantities needed for an understanding of nucleon and nuclear structure. The evolution of the electric and magnetic form factors with Q^2, the square of the four-momentum transfer, is related to the charge and current distributions within the nucleon. Precision measurements of the electromagnetic form factors are important for tests of nonperturbative quantum chromodynamics (QCD) either on the lattice or in models. With the advent of high duty-factor polarized electron beam facilities, experiments employing recoil polarimeters [1,2], polarized ^{3}He targets [3–5], and polarized deuterium targets [6,7] have yielded the first precision measurements of G_E^n, the neutron electric form factor. These polarization measurements of G_E^n are limited to $Q^2 \leq 0.67\ (\mathrm{GeV}/c)^2$ and are, within errors, consistent with the Galster parametrization [8].

In the plane-wave approximation, the recoil polarization produced by a longitudinally polarized electron beam in quasielastic electron-neutron scattering is restricted to the scattering plane [9,10]: The longitudinal component, $P_{L'}$, and the transverse (sideways) component, $P_{S'}$, are parallel and perpendicular, respectively, to the recoil neutron's momentum vector. In terms of G_E^n and G_M^n, $P_{S'}$ and $P_{L'}$ can be written as

$$P_{S'}/P_L = -K_S G_E^n G_M^n / I_0, \tag{1}$$

 0031-9007/03/91(12)/122002(5)\$20.00

$$P_{L'}/P_L = K_L(G_M^n)^2/I_0, \tag{2}$$

where P_L is the electron beam polarization, $I_0 \equiv (G_E^n)^2 + K_0(G_M^n)^2$, and K_S, K_L, and K_0 are kinematic functions of the electron scattering angle, θ_e, and Q^2. Measurements of $P_{S'}$ and $P_{L'}$ via a secondary analyzing reaction permit an extraction of the ratio of G_E^n to G_M^n; a significant advantage of this technique is that P_L and the analyzing power of the secondary reaction cancel in the polarization ratio $P_{S'}/P_{L'}$. Also, for quasifree emission, Arenhövel [11] demonstrated that $P_{S'}$ and $P_{L'}$ are insensitive to final state interactions (FSI), meson exchange currents (MEC), isobar configurations (IC), and to theoretical models of deuteron structure.

In this Letter, we report new measurements of G_E^n/G_M^n obtained via recoil polarimetry from the quasielastic $^2\mathrm{H}(\vec{e}, e'\vec{n})^1\mathrm{H}$ reaction at three central Q^2 values of 0.45, 1.15, and 1.47 $(\mathrm{GeV}/c)^2$. Our measurements were carried out in Hall C of the Thomas Jefferson National Accelerator Facility. The experimental arrangement with an isometric view of our polarimeter is shown in Fig. 1. A beam of longitudinally polarized electrons (with a typical polarization of 80%) scattered quasielastically from a neutron in a 15-cm liquid deuterium target. A scattered electron was detected in the High Momentum Spectrometer (HMS) in coincidence with the recoil neutron. The neutron polarimeter (NPOL) was used to measure the up-down scattering asymmetry from the transverse component of the recoil neutron polarization presented to the polarimeter. To permit measurements of the up-down scattering asymmetry from different combinations of $P_{S'}$ and $P_{L'}$, a dipole magnet (Charybdis) located in front of the polarimeter precessed the recoil neutron's polarization vector through an angle χ.

The polarimeter consisted of a total of 44 plastic scintillation detectors. To achieve luminosities of $\sim 3 \times 10^{38}\ \mathrm{cm}^{-2}\,\mathrm{s}^{-1}$, the front array was segmented into 20 detectors [100 cm × 10 cm × 10 cm]. Top and bottom rear arrays were shielded from the direct path of particles from the target. Each rear array consisted of six "20-in" detectors [101.6 cm × 50.8 cm × 10.16 cm] and six "10-in" detectors [101.6 cm × 25.4 cm × 10.16 cm]. A double layer of "veto/tagger" detectors (each 0.64-cm thick) directly ahead of and behind the front array identified incoming and scattered charged particles. A 10-cm lead curtain attenuated the flux of electromagnetic radiation and charged particles incident on the polarimeter. The flight path from the center of the target to the center of the front array was 7.0 m, and the mean flight path from the front array to the rear array was 2.5 m.

For a fixed neutron scattering angle of 46.0°, central Q^2 values of 0.45 and 1.47 $(\mathrm{GeV}/c)^2$ were associated with beam energies of 0.884 and 3.40 GeV, respectively, and electron scattering angles of 52.7° and 23.6°, respectively. The measurement conducted at a central Q^2 value of 1.15 $(\mathrm{GeV}/c)^2$ was associated with two beam energies of 2.33 and 2.42 GeV and electron scattering angles of 30.8° and 30.1°, respectively. We conducted asymmetry measurements with the polarization vector precessed through $\chi = \pm 40°$ at each of our Q^2 points; in addition, at $Q^2 = 1.15$ and 1.47 $(\mathrm{GeV}/c)^2$, we conducted asymmetry measurements with the polarization vector precessed through $\chi = 0°, \pm 90°$. The acceptance-averaged values of Q^2 are $\langle Q^2 \rangle = 0.45$, 1.13, and 1.45 $(\mathrm{GeV}/c)^2$.

Typical time-of-flight spectra are shown in Fig. 2. The left panel is an HMS-NPOL coincidence time-of-flight spectrum. We compared the measured time of flight, cTOF, with the time of flight calculated from electron kinematics and offsets determined by a calibration procedure; the result is centered on zero with a FWHM of approximately 1.5 ns. The right panel is the time-of-flight spectrum between a neutron event in the front array and an event in the top or bottom rear array. We compared this measured time of flight, ΔTOF, with the time of flight calculated for elastic np scattering. Variations with respect to a nominal 2.5 m flight path were compensated. The tail on the slow side is due to Fermi motion in carbon and nuclear reactions, and the secondary peak at ~ -2.5 ns is the result of π^0 production in the front array. To extract the physical scattering asymmetry, we calculated the cross ratio, r, which is defined to be the ratio of two geometric means, $(N_U^+ N_D^-)^{1/2}$ and

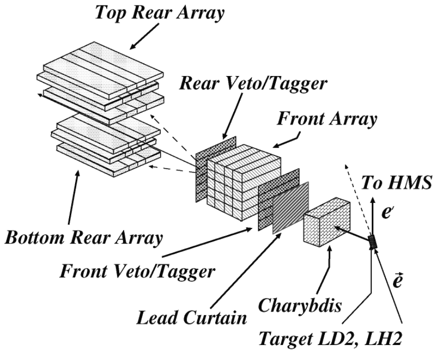

FIG. 1. A schematic diagram of the polarimeter.

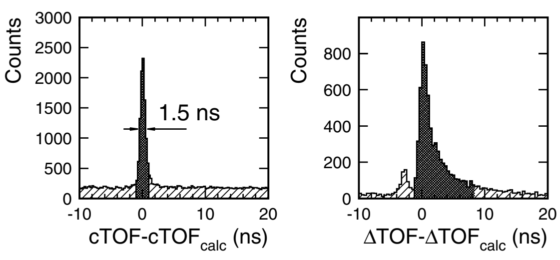

FIG. 2. Typical time-of-flight spectra for $Q^2 = 1.15\ (\mathrm{GeV}/c)^2$. Selected portions are shaded.

$(N_U^- N_D^+)^{1/2}$, where $N_U^+(N_D^-)$ is the yield in the ΔTOF peak for neutrons scattered up (down) when the beam helicity was positive (negative); the yields, corrected for background, were obtained by peak fitting. The physical scattering asymmetry is then given by $(r-1)/(r+1)$. The merit of the cross ratio technique [12] is that the neutron polarimeter results are independent of the luminosities for positive and negative helicities, and the efficiencies and acceptances of the top and bottom halves of the polarimeter. Beam charge asymmetries (of typically 0.1%) and detector threshold differences cancel in the cross ratio.

To account for the finite experimental acceptance and nuclear physics effects such as FSI, MEC, and IC, we averaged Arenhövel's theoretical $^2\mathrm{H}(\vec{e}, e'\vec{n})^1\mathrm{H}$ calculations [13] over the experimental acceptance. These calculations include leading-order relativistic contributions to a nonrelativistic model of the deuteron as an n-p system, employ the Bonn R-space NN potential [14] for the inclusion of FSI, and include MEC and IC. Other realistic potentials (e.g., the Argonne V18 [15]) give essentially the same results. Recoil polarizations were calculated over a kinematic grid; we used multidimensional interpolation to compute the polarizations between the grid elements.

To average these theoretical calculations over the experimental acceptance, we prepared two independent simulation programs. First, we developed the GENGEN Monte Carlo simulation program, which includes an event generator and detailed models of the electron spectrometer and the neutron polarimeter. GENGEN reproduces experimental kinematic distributions and models the response of the polarimeter. Second, we developed a program that used the kinematics of the reconstructed quasielastic events from the experimental data to compute the recoil polarization for each event used in the data analysis; the advantage of this method is that it does not require a model of the experimental acceptance.

For the first-pass analysis, the simulation programs used theoretical calculations that assumed the Galster parametrization for G_E^n with different multiplicative factors. We determined the optimal factor for each Q^2 that provided the best agreement between the simulated polarization ratios and the experimental asymmetry ratios. Next, we fitted the current world data [1,2,4–7,16,17] and our first-pass acceptance and nuclear physics corrected results for G_E^n to a Galster parametrization with two free parameters. Then we repeated the simulations using new theoretical calculations that assumed this modified Galster parametrization for G_E^n. As in the first-pass analysis, we determined the optimal factor that provided the best agreement between simulation and experiment. The differences between these analyses were negligible, and the results from the two simulation programs agreed to better than 2%.

TABLE I. Estimated systematic uncertainties in $\Delta g/g$ [%].

Source	$\langle Q^2 \rangle$ [(GeV$/c$)^2] 0.45[a]	1.13[a]	1.13[b]	1.45[a]	1.45[b]
Beam polarization	1.4	0.8	0.4	1.7	0.3
Charge exchange	<0.01	0.02	0.06	<0.01	0.2
Depolarization	<0.1	<0.1	0.2	0.1	0.6
Positioning/traceback	0.2	0.3	0.3	0.4	0.4
Precession angle	1.1	0.3	0.1	0.5	0.1
Radiative corrections	0.7	0.1	0.1	0.05	0.05
Total of above sources	1.9	0.9	0.5	1.8	0.8

[a] $\chi = \pm 40°$ precession.
[b] $\chi = 0°, \pm 90°$ precession.

The estimated values of the systematic uncertainties are listed in Table I. A significant advantage of our experimental technique is that the scale and systematic uncertainties are small; the analyzing power of the polarimeter cancels in the polarization ratio, and the beam polarization, P_L, also cancels as it varied little during sequential measurements of the scattering asymmetries. We measured the beam polarization with a Møller polarimeter [18], and changes in P_L were typically ~1%–2%. The helicity of the beam was reversed at a frequency of 30 Hz to eliminate instrumental asymmetries.

A false asymmetry or a dilution of the asymmetry may arise from the two-step process $^2\mathrm{H}(\vec{e}, e'\vec{n})^1\mathrm{H} + \mathrm{Pb}(\vec{p}, \vec{n})$; the contamination from this process was assessed by running with a liquid hydrogen target. The contamination levels are negligible ($\lesssim 0.3\%$) for $\chi = \pm 40°$ and $\pm 90°$ at all of our Q^2 points, and for $\chi = 0°$, the contamination levels are ~0.3% and ~3% at $\langle Q^2 \rangle = 1.13$ and 1.45 (GeV$/c$)^2, respectively; accordingly, we have not corrected our $\langle Q^2 \rangle = 0.45$ and 1.13 (GeV$/c$)^2 data for contamination from this two-step process. The net correction obtained for the analysis of all of the data for $\langle Q^2 \rangle = 1.45$ (GeV$/c$)^2 [viz., for $\chi = 0°$, $\pm 40°$, and $\pm 90°$] amounted to 1.3% ± 0.1%. In addition to charge-exchange reactions in the lead curtain, the flux of neutrons entering the polarimeter may be depolarized as a result of nuclear interactions in the lead curtain.

TABLE II. Results for $g = G_E^n/G_M^n$ and G_E^n. [The first set of errors is statistical, and the second set is systematic.]

$\langle Q^2 \rangle$ [(GeV$/c$)^2]	$g = G_E^n/G_M^n$	$G_M^n/\mu_n G_D$ [20]	G_E^n
0.447	$-0.0761 \pm 0.0083 \pm 0.0021$	1.003 ± 0.006	$0.0550 \pm 0.0060 \pm 0.0016$
1.132	$-0.131 \pm 0.010 \pm 0.003$	1.057 ± 0.017	$0.0394 \pm 0.0029 \pm 0.0012$
1.450	$-0.190 \pm 0.016 \pm 0.004$	1.044 ± 0.024	$0.0411 \pm 0.0035 \pm 0.0013$

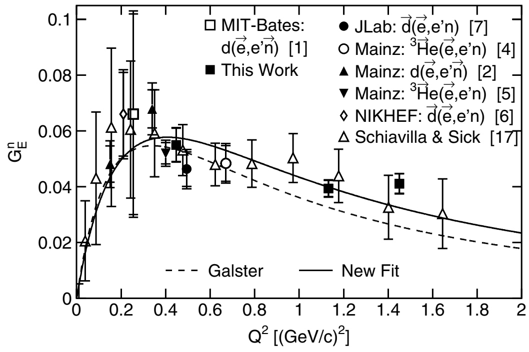

FIG. 3. The current world data on G_E^n versus Q^2 extracted from polarization measurements and an analysis of the deuteron quadrupole form factor [1,2,4–7,17].

Depolarization processes were simulated in GENGEN using a spin-dependent multiple-scattering algorithm employing quasifree scattering from a Fermi gas. The effects of depolarization cancel in the polarization ratio, and the residual noncancellation effect upon g of less than 0.6% is included in the systematic uncertainty.

Afanasev *et al.* [19] calculated radiative corrections to the polarization-transfer coefficients, $P_{S'}/P_L$ and $P_{L'}/P_L$. The primary effect is depolarization of the electron such that both polarization-transfer coefficients should be increased by ~1.9%, ~3.7%, and ~4.4% at $\langle Q^2 \rangle = 0.45$, 1.13, and 1.45 (GeV$/c)^2$, respectively; however, these effects nearly cancel in the polarization ratio such that the net effect upon g is small at $\langle Q^2 \rangle = 0.45$ (GeV$/c)^2$ and negligible at the two higher Q^2 points.

The values of g and G_E^n that we report are listed in Table II. To determine our values for G_E^n, we used the best-fit values for G_M^n (listed in Table II) obtained using the methods described in [20]. The quoted systematic uncertainties include a 2% uncertainty that results when different data are used for the time calibration.

Our values for G_E^n are plotted in Fig. 3 together with the current world data on G_E^n [1,2,4–7,17] extracted from polarization measurements and an analysis of the deuteron quadrupole form factor [17]. We fitted these data and the G_E^n slope at the origin as measured via low-energy neutron scattering from electrons in heavy atoms [16] to a Galster parametrization: $G_E^n = -a\mu_n \tau G_D/(1 + b\tau)$, where $\tau = Q^2/4M_n^2$, $G_D = (1 + Q^2/\Lambda^2)^{-2}$, and $\Lambda^2 = 0.71$ (GeV$/c)^2$. Our best-fit parameters are $a = 0.888 \pm 0.023$ and $b = 3.21 \pm 0.33$.

Polarization measurements of G_E^p/G_M^p [21–24] and G_E^n/G_M^n [1,2,4–7,17] are compared with predictions of selected models in Fig. 4. The chiral soliton model [25] reproduces the dramatic linear decrease observed in $\mu_p G_E^p/G_M^p$ for $1 < Q^2 < 6$ (GeV$/c)^2$; however, this model fails to reproduce the neutron data at large Q^2. The light-cone diquark model [26] achieves qualitative

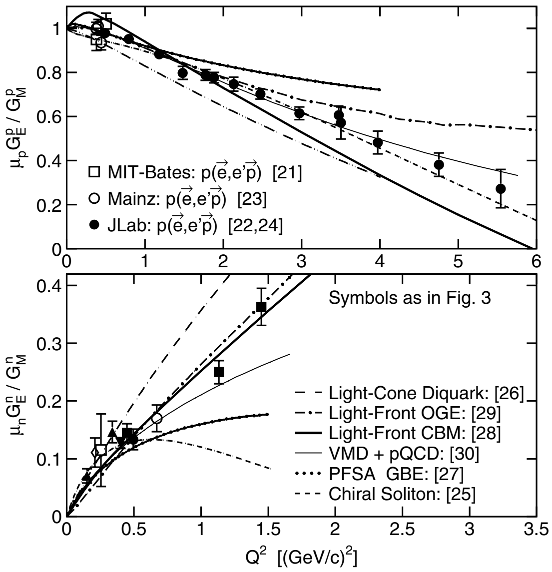

FIG. 4. Predictions of selected models (see text) for $\mu_p G_E^p/G_M^p$ and $\mu_n G_E^n/G_M^n$ compared with proton [21–24] and neutron [1,2,4–7] data.

agreement with the low Q^2 proton and neutron data; however, at high Q^2, it lies below (above) the proton (neutron) data. A calculation using the pointform spectator approximation (PFSA) with pointlike constituent quarks and a Goldstone boson exchange interaction fitted to the meson and baryon spectrum [27] also achieves qualitative agreement with the low Q^2 proton and neutron data; however, it also fails to describe the high Q^2 proton and neutron data. A light-front calculation using pointlike constituent quarks surrounded by a cloud of pions [28] describes the neutron data, but falls below the proton data at high Q^2. A one-gluon exchange light-front calculation using constituent quark form factors fitted to $Q^2 < 1$ (GeV$/c)^2$ data [29] agrees with the neutron data, but deviates from the proton data above $Q^2 \sim 3.5$ (GeV$/c)^2$. Finally, fits that couple vector meson dominance with the predictions of perturbative QCD [30] agree with the entire range of the proton data, but fall below the neutron data above $Q^2 \sim 1.2$ (GeV$/c)^2$.

A successful model of confinement must be able to predict both neutron and proton electromagnetic form factors simultaneously. The neutron electric form factor is especially sensitive to small components of the nucleon wave function, and differences between model predictions for G_E^n tend to increase rapidly with Q^2. Our new G_E^n data provide a challenging test for confinement models and invite extensions to higher Q^2.

We thank the TJNAF Hall C scientific and engineering staff for their outstanding support. Also, we thank A. Afanasev for providing calculations of the radiative correction uncertainties. This work was supported in part by the National Science Foundation, the U.S. Department of Energy, and the Deutsche Forschungsgemeinschaft. The Southeastern Universities Research Association (SURA) operates the Thomas Jefferson National Accelerator Facility under the U.S. Department of Energy Contract No. DE-AC05-84ER40150.

*Present Address: Renaissance Technologies, 600 Route 25A, East Setauket, New York 11733, USA.
†Present Address: Department of Physics and Astronomy, University of Canterbury, Private Bag 4800, Christchurch 8020, New Zealand.
‡Present Address: Atmospheric Chemistry Division, National Center for Atmospheric Research, Boulder, Colorado 80307, USA.

[1] T. Eden *et al.*, Phys. Rev. C **50**, R1749 (1994).
[2] C. Herberg *et al.*, Eur. Phys. J. A **5**, 131 (1999) applies FSI corrections to M. Ostrick *et al.*, Phys. Rev. Lett. **83**, 276 (1999).
[3] M. Meyerhoff *et al.*, Phys. Lett. B **327**, 201 (1994).
[4] J. Bermuth *et al.*, Phys. Lett. B **564**, 199 (2003) updates D. Rohe *et al.*, Phys. Rev. Lett. **83**, 4257 (1999).
[5] J. Golak, G. Ziemer, H. Kamada, H. Witala, and W. Glöckle, Phys. Rev. C **63**, 034006 (2001) applies FSI corrections to J. Becker *et al.*, Eur. Phys. J. A **6**, 329 (1999).
[6] I. Passchier *et al.*, Phys. Rev. Lett. **82**, 4988 (1999).
[7] H. Zhu *et al.*, Phys. Rev. Lett. **87**, 081801 (2001).
[8] S. Galster, H. Klein, K. H. Schmidt, D. Wegener, and J. Bleckwenn, Nucl. Phys. B **32**, 221 (1971).
[9] A. I. Akhiezer and M. P. Rekalo, Sov. J. Part. Nuclei **4**, 277 (1974).
[10] R. G. Arnold, C. E. Carlson, and F. Gross, Phys. Rev. C **23**, 363 (1981).
[11] H. Arenhövel, Phys. Lett. B **199**, 13 (1987); H. Arenhövel (private communication).
[12] G. G. Ohlsen and P. W. Keaton, Jr., Nucl. Instrum. Methods **109**, 41 (1973).
[13] H. Arenhövel, W. Leidemann, and E. L. Tomusiak, Phys. Rev. C **52**, 1232 (1995); **46**, 455 (1992); Z. Phys. A **331**, 123 (1988); **334**, 363(E) (1989); H. Arenhövel (private communication).
[14] R. Machleidt, K. Holinde, and Ch. Elster, Phys. Rep. **149**, 1 (1987).
[15] R. B. Wiringa, V. G. J. Stoks, and R. Schiavilla, Phys. Rev. C **51**, 38 (1995).
[16] S. Kopecky *et al.*, Phys. Rev. C **56**, 2229 (1997); Phys. Rev. Lett. **74**, 2427 (1995).
[17] R. Schiavilla and I. Sick, Phys. Rev. C **64**, 041002 (2001).
[18] M. Hauger *et al.*, Nucl. Instrum. Methods Phys. Res., Sect. A **462**, 382 (2001).
[19] A. Afanasev, I. Akushevich, and N. Merenkov, Phys. Rev. D **64**, 113009 (2001).
[20] J. J. Kelly, Phys. Rev. C **66**, 065203 (2002).
[21] B. D. Milbrath *et al.*, Phys. Rev. Lett. **80**, 452 (1998); **82**, 2221(E) (1999).
[22] M. K. Jones *et al.*, Phys. Rev. Lett. **84**, 1398 (2000); V. Punjabi *et al.* (to be published).
[23] Th. Pospischil *et al.*, Eur. Phys. J. A **12**, 125 (2001).
[24] O. Gayou *et al.*, Phys. Rev. Lett. **88**, 092301 (2002).
[25] G. Holzwarth, hep-ph/020138; Z. Phys. A **356**, 339 (1996). [Version B2 is shown in Fig. 4.]
[26] B.-Q. Ma, D. Qing, and I. Schmidt, Phys. Rev. C **65**, 035205 (2002).
[27] S. Boffi, L. Ya. Glozman, W. Klink, W. Plessas, M. Radici, and R. F. Wagenbrunn, Eur. Phys. J. A **14**, 17 (2002); M. Radici (private communication).
[28] G. A. Miller, Phys. Rev. C **66**, 032201(R) (2002); G. A. Miller (private communication).
[29] F. Cardarelli and S. Simula, Phys. Rev. C **62**, 065201 (2000); S. Simula (private communication).
[30] E. L. Lomon, Phys. Rev. C **66**, 045501 (2002); **64**, 035204 (2001).